Received: 16 April 2020 | Revised: 12 July 2020 | Accepted: 14 July 2020

DOI: 10.1002/aoc.5953

FULL PAPER

Applied Organometallic Chemistry WILEY

Synthesis, molecular modeling, TD-DFT, antimicrobial, and in vitro therapeutic activity of new spherical nano-sized sulfonamide imine ligands and their zinc (II) and copper (II) complexes

Ali El-Dissouky[1] | Eslam S. Abu-Elsoud[1] | Afaf Abdel Razik[1] | Mohamed K. Awad[2] | Hammed H.A.M. Hassan[1] | Amel F. Elhusseiny[1]

[1]Chemistry Department, Faculty of Science, Alexandria University, 2 Bagdad street, PO Box 2-Moharrem Beck, Alexandria, 21321, Egypt

[2]Theoretical Applied Chemistry Unit (TACU), Chemistry Department, Faculty of Science, Tanta University, Tanta, Egypt

Correspondence
Amel F. Elhusseiny, Chemistry Department, Faculty of Science, Alexandria University, 2 Bagdad street, PO Box 2-Moharrem Beck, 21321 -Alexandria, Egypt.
Email: amel_elhusseiny@sci.alexu.edu.eg

A series of nanometer-sized spherical sulfonamide imine ligands **HL[1]-HL[5]** and their copper and zinc complexes were synthesized and fully characterized based on elemental analyses, spectroscopic (U*V*/vis, FT-IR, NMR, EPR, SEM) studies, molar conductance and thermal analyses. Furthermore, computational studies of **HL[1]-HL[5]** were carried out by the DFT/B3LYP method. TD-DFT, HOMO and LUMO energy values, chemical hardness, electronegativity, electrophilic index, softness, and other parameters were calculated. Screening against several pathogenic microorganisms indicated that **HL[1]** exhibited high activity against the tested Gram-negative bacteria relative to other analogues and the inhibition activity is greater than the standard *Gentamicin*. Analogously, **HL[2]** exhibited high potent activity against the tested Gram-positive bacteria. Copper complexes exhibited a higher potent activity than zinc analogues. Noteworthy, inhibition activity of [Cu (**L[3]**)(OAc)] complex is higher than that of the standard *Ampicillin*. [Cu (**L[2]**)(OAc)] complex displayed a similar activity of the standard bactericides and fungicides in use. The complexes showed appreciated values of MIC against bacterial strains: *B. subtilis* (MIC = 0.4 μg / mL), *E. coli* and *S. pneumonia* (MIC = 1.95 μg / mL) and *P. aeruginosa* (MIC = 7.81 μg / mL). in vitro cytotoxic activities study proved that [Cu (**L[3]**)(OAc)] complex exhibited appreciable activity versus (HEPG-2); IC_{50} = 4.8 μg/ml, while [Cu(**L[2]**)(OAc)] complex showed a high activity against (MCF-7); IC_{50} = 6.2 μg/ml. These results could be considered as new findings of promising antitumor candidates for experimental chemotherapy.

KEYWORDS

complexes, computational studies, cytotoxicity, nanomaterial, spectroscopic

1 | INTRODUCTION

Sulfa-drugs are ligands possess potent biological activity because of their crucial role in eliminating a wide range of human infections and many animal systems.[1] Their chemical structures, enriched with nitrogen, sulfur and oxygen groups, offered a great tendency to form metal complexes. Chemical modification by reaction with

varieties of aldehydes, ketones or chelation with metals furnished biologically active and powerful corrosion inhibitors.[1–4]

The copper and zinc ions were described as ions of interest for several biological processes.[5] These ions are key factors in cellular metabolism and activate many critical enzymes functions in protein and DNA syntheses.[6] Their coordination modulated protein structures for clarifying biological function and occurred as a core factor in protein revenue and misfolding of protein- illnesses.[7] Furthermore, these ions possess antioxidant and pro-antioxidant properties against accelerated ageing and injury healing.[8] As an antioxidant, copper scavenges free radicals and diminish their damage effect.[9] As a pro-oxidant, on the contrary, it supports free radical damage and adds to the advance of Alzheimer's sickness.[10] Zinc ions are active antimicrobial agents even at low concentrations. It may be a neurotoxin, proposing zinc homeostasis showing a serious role in normal brain operations and central nervous system.[11] Cu proteins have different characters in biological electron transport and oxygen transportation triggering easy Cu(I) → Cu (II) interexchange. Copper is essential for phospholipids production found in peripheral nerves.[12]

The use of inherently nanostructured bioactive materials for nanotherapy is an encouraging method for future active chemotherapy. Many organic materials could be prepared in a quite precise way to form various nanoscale structures down to the molecular scale. Such nanomaterials could be synthesized either by interfacial techniques or by emulsion method. A commonly used method for organic nanoscale materials preparation is solvent displacement referred to nanoprecipitation.[13] This method includes the dissolution of the monomers in an organic, water-miscible solvent, which is then added to the aqueous phase in the presence or absence of a surfactant. In addition to the aqueous phase, the organic solvent instantly spreads out leading to the development of nanoscale materials.

In the current study, we present (i) the preparation and characterization of new nanosized sulfonamide-imine ligands, Figure 1, namely; 4-{[(1E)-(2-hydroxy-1-salicyl)methylene]-amino}-*N*-(4,6-dimethyl pyrimidin-2-yl)benzenesulfonamide (**HL^1**), 4-{[(1E)-(2-hydroxy-1-salicyl)methylene]-amino}-*N*-(4-methyl pyrimidin-2-yl) benzene sulfonamide (**HL^2**), 4-{[(1E)-(2-hydroxy-1-naphthyl)methylene]amino}-*N*-(4,6-dimethylpyrimidin-2-yl) benzenesulfonamide (**HL^3**), 4-{[(1E)-(2-hydroxy-1-naphthyl) methylene]amino}-*N*-(4-methyl pyrimidin-2-yl)benzenesulfon amide (**HL^4**) and 4-{[(1E)-(2-hydroxy-1-naphthyl)methylene]amino} -*N*-pyrimidin-2-yl) benzenesulfonamide (**HL^5**). (ii) the TD-DFT calculations

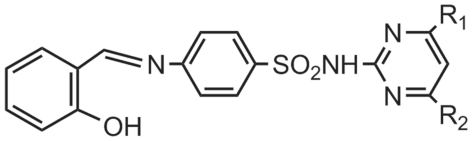

HL^1: R$_1$ = R$_2$ = CH$_3$
HL^2: R$_1$ = H, R$_2$ = CH$_3$

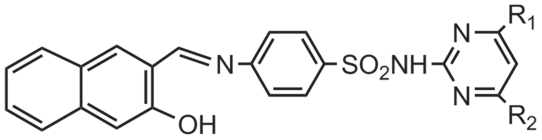

HL^3: R$_1$ = R$_2$ = CH$_3$
HL^4: R$_1$ = H, R$_2$ = CH$_3$
HL^5: R$_1$ = R$_2$ = H

FIGURE 1 Structures of the sulfonamide imines **HL^1-HL^5**

to understand the structure of the ligands, upon using geometry optimization and HOMO-LUMO analysis. (iii) the synthesis and the characterization of their copper and zinc complexes. (iv) the evaluation of in-vitro bactericidal and fungicidal activities of all the prepared compounds and the Minimum Inhibitory Concentration (MIC) activities against a panel of microorganisms. (v) the study of in vitro cytotoxicity and the IC_{50} versus the selected mammalian cell lines, breast cancer (MCF7), liver cancer (HEPG2), and colon cancer (HCT116).

2 | EXPERIMENTAL

2.1 | Materials and solvents

4-amino-*N*-(4,6-dimethylpyrimidin-2-yl) benzenesulfonamide (sulfamethazine), 4-amino-*N*-(4-methyl pyrimidin-2-yl) benzenesulfonamide (sulfamerazine), 4-amino-*N*-(pyrimidin-2-yl) benzene sulfonamide (sulfadiazine), salicylaldehyde and 2-hydroxynaphthaldehyde were purchased from Aldrich. Ethanol (BDH-PROLABO), dimethyl sulfoxide (DMSO, Aldrich) and diethyl ether were of pure grade quality and used as received. Hydrated divalent copper and zinc acetates were purchased from Aldrich and used as received.

2.2 | Physical measurements

Microanalyses of carbon, hydrogen, nitrogen, and sulfur were carried out at the Regional Centre of Mycology and Biotechnology, El-Azhar University, Cairo. The metal analysis was performed by the atomic absorption technique, Faculty of Science, Alexandria University, in

SCHEME 1 Synthesis of sulfonamide imine ligands **HL^1- HL^5** and their Cu (II) and Zn (II) complexes.>

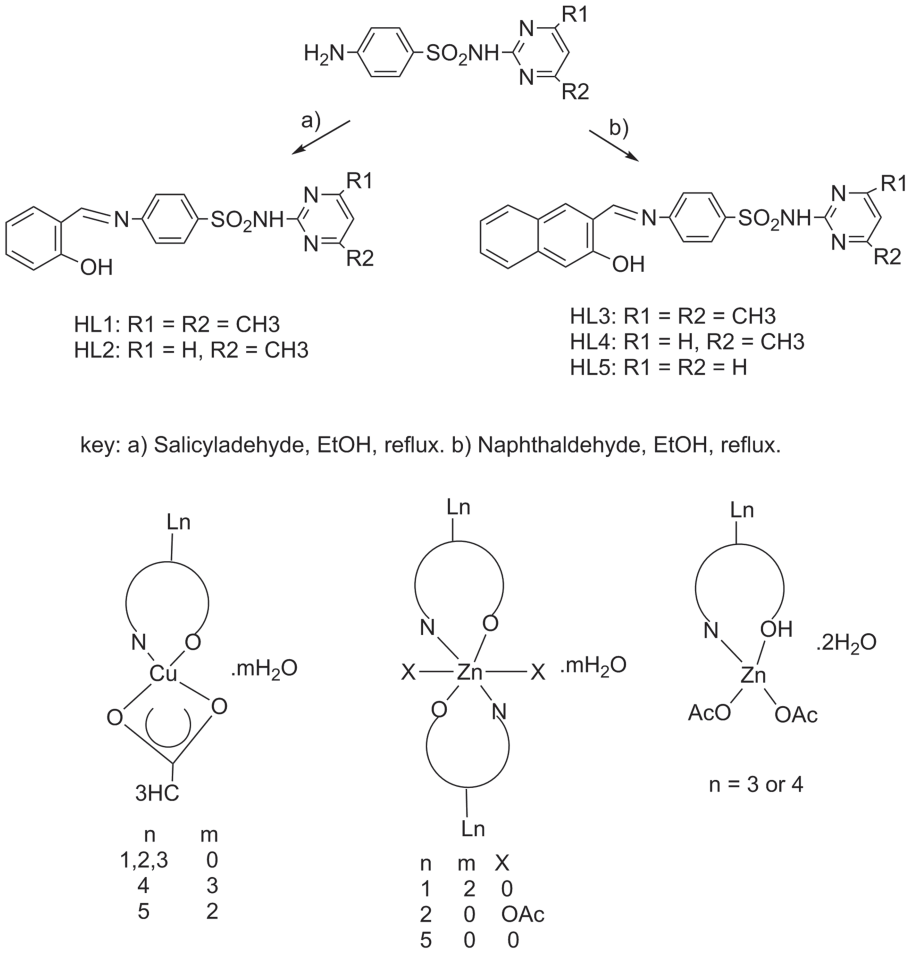

addition to complexometric titration using standard EDTA solution in the presence of a suitable metal indicator at the appropriate pH. The melting points of the prepared compounds were measured using an electro-thermal melting point apparatus and were not corrected. FT-IR spectra (KBr pellets; 3 mm thickness) were carried out on a Perkin-Elmer FT-IR Spectrophotometer (FT-IR 1650). All spectra were recorded within the wavenumber range of 4,000–500 cm^{-1} at room temperature 25 ± 1 °C. Electronic spectra were performed using a UV 500 UV–vis spectrophotometer at room temperature (RT) as dimethyl sulphoxide solutions. The ^{1}H-NMR spectra were carried out on a JEOL 500 spectrometer as DMSO-d6 solution with TMS as an internal standard at Faculty of Science Alexandria University. Molar conductivity measurements were measured using HI 8033 HANNA conductometer at 25 ± 1 °C for 10^{-3} M DMSO solution. Digital Orion pH/ISE meter was used for the pH measurements. EPR measurements on polycrystalline copper samples were measured at room temperature 298 K using a high sensitivity standard cylindrical resonator (ER 4119HS) operating at 9.8 GHz, with a 100 kHz modulation frequency and DPPH as an external standard at National Institute for standards–Giza-Egypt. Thermal analyses were recorded in the temperature range from 25 °C to 1,000 °C using LINSEIS STA PT1000 thermogravimetric analyzer. The experimental conditions were as follows: the platinum crucible and the heating rate were 10 °C/min. and the maximum sample weight was 10 mg, at the central laboratory unit, Faculty of Science, Alexandria University. The morphologies of nanosized organic ligands were detected by Scanning Electron Microscope (SEM) (JEOL-JSM5300), at the E-Microscope Unit; Faculty of Science, Alexandria University. Sonication of samples was done in de-ionized water for 5 min, then deposited onto a carbon-coated copper mesh and allowed to air-dry before the examination. Antimicrobial Screening tests and Cytotoxicity studies were accomplished at the Regional Centre of Mycology and Biotechnology, El-Azhar University, Cairo.

2.3 | Synthesis of organic ligands HL^1-HL^5 (general method)

The organic ligands **HL^1-HL^5** were synthesized according to the reported procedure with a slight modification.[14,15] The aldehydes namely; salicylaldehyde

(0.4 mL, 3.50 mmol) or 2-hydroxy-1-naphthaldehyde (0.6 g, 3.7 mmol) dissolved in absolute ethanol(25 mL) was added to a warm solution of the appropriate sulfonamides (3.50 mmol) namely: Sulfamethazine(1.0 g), sulfamerazine(0.94 g) or sulfadiazine (0.87 g) in absolute ethanol (15 mL). The mixture was acidified with drops of glacial acetic acid followed by reflux for four hours. After the mixture was cooled, the orange solid product was isolated and recrystallized from ethanol. The recrystallized precipitate was isolated by filtration, washed with ethanol, ether and dried under vacuum at 60 °C for 24 h and then kept in a vacuum desiccator. The compounds were checked for purity by TLC and their sharp melting points

2.3.1 | 4-{[(1E)-(2-Hydroxy-1-salicyl) methylene]-amino}-*N*-(4,6-dimethyl pyrimidin-2-yl) benzenesulfonamide (HL^1)

Yield 95.4%; m.p. 265 °C; yellow solid. Anal. Calc. for $C_{19}H_{18}N_4SO_3$ (%): C, 59.6; H, 4.70; N, 14.6; S, 8.3. Found (%): C, 59.5; H, 4.4; N, 14.6; S, 8.5; FT-IR (ν, cm^{-1}): 3393, 1,595, 1,238, 1,310, 1,149. UV–Vis (λmax, nm): 260, 355, 400. ^{1}H-NMR (δ, ppm): Four CH_3 protons signals at δ 2.23 ppm, 2.20 ppm, 2.28 ppm, 2.26 ppm., CH=N proton at δ 8.93 ppm, δ 8.90 ppm, δ 8.89 ppm. Deuteratable broad singlet signal at δ 5.21 ppm NH proton. The aromatic protons δ 6.57–6.49 (m, 1H), δ 6.64–6.62 (m, 1H), δ 6.72–6.65 (m, 1H), δ 6.84–6.80 (m, 1H), δ 7.03–6.87 (m, 1H), δ 7.43–7.38 (m, 1H), δ 7.50–7.46 (m, 1H), δ 7.77–7.55 (m, 1H), δ 8.03–8.01 (m, 1H) and δ 8.17–8.08 (m, 1H).

2.3.2 | 4-{[(1E)-(2-Hydroxy-1-salicyl) methylene]-amino}-*N*-(4-methylpyrimidin-2-yl) benzene sulfonamide (HL^2)

Yield 96%; m.p. 180 °C; yellow solid. Anal. Calc. for $C_{18}H_{16}N_4SO_3$ (%): C, 58.6; H, 4.30; N, 15.2; S, 8.6. Found (%): C, 58.6; H, 4.2; N, 15.4; S, 8.8; FT-IR(ν, cm^{-1}): 3436, 1,594, 1,340, 1,245, 1,160.. UV–Vis (λmax, nm): 260,355, 400. ^{1}H-NMR (δ, ppm): Broad singlet OH signal at δ11.77 ppm, two singlet signals at δ10.14 and δ10.13 corresponding to 1H and aromatic protons resonated at δ 8.86 ppm (2 s δ 8.24–8.22 ppm (m) δ 8.0 ppm (m), δ7.66–7.60 (m) δ7.54–7.48 (m), δ7.47–7.42 (m), δ6.99–6.94 (m) δ6.86–6.83 (m), δ6.58–6.55 (m), δ2.27 (s, 3H, major), δ 2.29 (s, 3H, minor).

2.3.3 | 4-{[(1E)-(2-Hydroxy-1-naphthyl) methylene]amino}-*N*-(4,6-dimethylpyrimidin-2-yl) benzenesulfonamide (HL^3)

Yield 80.5%; m.p. 237 °C; yellow solid. Anal. Calc. for $C_{23}H_{20}N_4SO_3$ (%): C, 63.8; H, 4.60; N, 12.9; S, 7.4. Found (%): C, 63.7; H, 4.3; N, 12.7; S, 7.1; FT-IR(ν, cm^{-1}): 3444, 1,589, 1,350, 1,245, 1,153. UV–Vis (λmax, nm): 260, 320, 420. ^{1}H-NMR (δ, ppm): Singlet OH signal at δ11.72, two singlets at δ 9.65 and δ 9.64, aromatic protons at δ 8.74, δ 8.72, δ 8.29–8.26 ppm (m), δ 8.09–8.02 (m), δ 7.87–7.82 (m), δ 7.70–7.65 (m), δ 7.63–7.62 (mδ7.61–7.60 (m), δ 7.59–7.58 (mδ7.56–7.50 (m), δ7.42–7.37 (m), δ 7.18–7.15 (m), δ6.88–6.85 (m), δ 6.68–6.66 (m), δ 6.58–6.55 (m), δ 2.23 (s, 3H, majorδ 2.20 (s, 3H, CH_3, minor).

2.3.4 | 4-{[(1E)-(2-Hydroxy-1-naphthyl) methylene]amino}-*N*-(4-methyl pyrimidin-2-yl) benzene sulfonamide (HL^4)

Yield 96.4%; m.p. 247 °C; yellow solid. Anal. Calc. for $C_{22}H_{18}N_4SO_3$ (%): C, 63.1; H, 4.3; N, 13.3; S, 7.6. Found (%): C, 63.3; H, 4.5; N, 13.6; S, 7.7; FT-IR(ν, cm^{-1}): 3436, 1,570, 1,338, 1,245, 1,151. UV–Vis (λmax, nm): 260, 320, 420. ^{1}H-NMR (δ, ppm): Broad deuteratable OH at δ 11.73, δ 9.57 (s, 1H, H1), δ 8.43 (d, j 9.0 Hz, 1H, arom), δ 8.31 (d, j 6.0 Hz, 1H, arom), δ 8.07 (2d, *j* 8.7 Hz, 6 Hz, 1H, arom), δ7.93 (d, *j* 9.0 Hz, 1H, arom), δ 7.74 (2d, *j* 6.2 Hz, 6.4 Hz, 2H, arom), δ 7.55 (2d, *j* 7.8, 7.8 Hz, 1H, arom), δ 7.36 (2d, *j* 7.2 Hz, 7.8 Hz, 2H, arom), δ 7.00 (d, *j* 9.3 Hz, 1H, arom), δ 6.91 (2d, *j* 5.1 Hz, 1H, arom), δ 2.32 (s, 3H, CH_3).

2.3.5 | 4-{[(1E)-(2-hydroxy-1-naphthyl) methylene]amino}-*N*-pyrimidin-2-yl) benzene sulfonamide (HL^5)

Yield 96.3%; m.p. 291 °C; yellow solid. Anal. Calc. for $C_{21}H_{16}N_4SO_3$ (%): C, 62.3; H, 3.9; N, 13.8; S, 7.9. Found (%): C, 62.1; H, 4.1; N, 14.2; S, 8.1; FT-IR(ν, cm^{-1}): 3436, 1,570, 1,338, 1,245, 1,151. UV–Vis (λmax, nm): 260, 320, 420. ^{1}H-NMR (δ, ppm): Singlet broad deuteratable OH at δ11.83, δ9.59 (s, 1H), aromatic protons resonated at δ.51 (d, *j* 6.6 Hz, 1H), δ.45 (d, *j* 8.7 Hz, 1H), δ.03 (d, *j* 8.7 Hz, 1H), δ7.93 (d, *j* 9.3 Hz, 1H), δ7.76 (2d, *j* 7.2 Hz, 8.4 Hz, 2H), δ 7.60 (d, *j* 6.0 Hz, 1H), δ7.52 (2d, *j* 7.2 Hz, 7.2 Hz, 2H), δ7.35 (2d, *j* 7.2 Hz, 7.8 Hz, 2H), δ 7.06 (2d, *j* 4.8 Hz, 4.8 Hz, 2H), δ 6.96 (2d, *j* 9.0 Hz, 1H), δ 6.56 (2d, *j* 9.0 Hz, 1H).

2.4 | Synthesis of nanosized organic ligand HL^1–HL^5 (general method)

Salicylaldehyde or 2-hydroxylnaphthaldehyde (0.5 mmol) dissolved in dioxane (50 mL) was added instantly to the appropriate sulfonamide drug namely; sulfamethazine, sulfamerazine or sulfadiazine (0.5 mmol) dissolved in dioxane/H_2O mixture (50: 5 *v*/v) in an ultrasonic bath. Few drops of glacial acetic acid were added to the solution and the turbid solution was further ultrasonicated at 42 KHz for a period of 1 h. The resulted colloidal solution was extracted by centrifugal separation for 15 min at 6000 rpm and the precipitate was thoroughly washed with water, ether and dried at 60 °C for 24 h in a vacuum oven.

2.5 | Synthesis of metal (II) complexes (general method)

A warm ethanolic solution of M $(OAc)_2.nH_2O$ [M = Cu (II) or Zn (II), n = 1 or 2, respectively] (2.0 mmol) was added to a (2.0 mmol) of the prepared organic ligands **HL^1-HL^5** in ethanol (25 mL). The mixture was refluxed for 2 h and the formed precipitate in each case was collected by filtration, washed thoroughly with ethanol, diethyl ether and dried at 60 °C for 24 h in a vacuum oven. The melting points of the synthesized complexes were in the range 219 °C to > 300 °C.

2.5.1 | [cu (L^1) (OAc)]

Yield 89.2%; m.p. 219 °C; brown solid. Anal. Calc. for $C_{21}H_{20}N_4SO_5Cu$ (%): C, 50.0; H, 3.9; N, 11.1; S, 6.3; Cu, 12.6. Found (%): C, 50. 3; H, 3.7; N, 11.4; S, 6.6; Cu, 12.7. Λm ($\Omega^{-1}mol^{-1}cm^2$) = 4; FT-IR (ν, cm^{-1}): 3398, 1,656, 1,517, 1,487, 1,340, 1,256, 1,167, 540,425. UV–Vis (λmax, nm): 265, 360, 430, 756.ESR: g_1 = 2.02, g_2 = 2.22, g_3 = 2.26; R_r = 0.12; <g> = 2.18

2.5.2 | [Zn (L^1) $_2$].2H_2O

Yield 90%; m.p. 240 °C; yellow solid. Anal. Calc. for $C_{38}H_{38}N_8S_2O_8Zn$(%): C, 52.8; H, 4.4; N, 12.9; S, 7.4; Zn, 7.5. Found (%): C, 53.1; H, 4.1; N, 13.3; S, 6.6; Zn, 7.4. Λm ($\Omega^{-1}mol^{-1}cm^2$) = 4; FT-IR (ν, cm^{-1}): 3387, 1,512, 1,374,1,271, 1,140, 586,452. UV–Vis (λ_{max}, nm): 270, 370, 430, ^{1}HNMR: CH=N δ10.05(s, 1H), NH δ5.96 (s,1H), CH_3 δ2.4 (s 6H), pyrimidin proton at δ 6.54(s,1H),aromatic protons δ6.70–7.74 (m, 8H).

2.5.3 | [cu (L^2)(OAc)]

Yield 94%; m.p. >300 °C; green solid. Anal. Calc. for $C_{20}H_{18}N_4SO_5Cu$ (%): C, 49.0; H, 3.6; N, 11.4; S, 6.5; Cu, 12.9. Found (%): C, 49. 2; H, 3.4; N, 11.6; S, 6.7; Cu, 12.9. Λm ($\Omega^{-1}mol^{-1}cm^2$) = 2; FT-IR (ν, cm^{-1}): 3444, 1,607, 1,567, 1,410, 1,339, 1,278, 1,161, 505, 446. UV–Vis (λmax, nm): 260, 320, 415, 700.ESR: g_1 = 2.05, g_2 = 2.14, g_3 = 2.26; R_r = 0.57; <g> = 2.15.

2.5.4 | [Zn (HL^2) $_2$ ($OAc)_2$]

Yield 95.2%; m.p. 231 °C; yellow solid. Anal. Calc. for $C_{40}H_{38}N_8S_2O_{10}Zn$ (%): C, 52.3; H, 3.9; N, 12.2; S, 6.9; Zn, 7.1. Found (%): C, 52.6; H, 4.1; N, 12.4; S, 7.2; Zn, 7.0. Λm ($\Omega^{-1}mol^{-1}cm^2$) = 3; FT-IR (ν, cm^{-1} [1)]: 1569, 1,245, 3,437, 1,158, 1,338, 1,490, 1,692, 506,439. UV–Vis (λmax, nm): 260, 320, 425, **^{1}HNMR:** CH=N δ8.60 (s, 1H),OH δ12.65 (s, 1H disappeared with D_2O),NH δ5.94(s,1H),CH_3 δ2.50 (s 6H), CH_3COO δ3.30(s, 6H),Pyrimidin protonδ 6.56 (m,2H),Aromatic protons δ6.60–7.98 (m, 8H**).**

2.5.5 | [cu (L^3) (OAc)]

Yield 90%; m.p. >300 °C; green solid. Anal. Calc. for $C_{25}H_{22}N_4SO_5Cu$ (%): C, 54.2; H, 3.9; N, 10.1; S, 5.7; Cu, 11.4. Found (%): C, 54. 9; H, 4.2; N, 10.3; S, 5.9; Cu, 12.7. Λm ($\Omega^{-1}mol^{-1}cm^2$) = 2; FT-IR (ν, cm^{-1}): 3458, 1,630, 1,535, 1,451, 1,368, 1,285, 1,138, 550, 437. UV–Vis (λmax, nm): 260, 320, 420, 690, ESR: $g_{\|}$=2.27, $g_{\perp}$=2.07; <g> = 2.13.

2.5.6 | Zn[(HL^3) ($OAc)_2$].2H_2O

Yield 89.2%; m.p. >300 °C; yellow solid. Anal. Calc. for $C_{27}H_{30}N_4SO_9Zn$ (%): C, 49.8; H, 4.4; N, 8.6; S, 4.9; Zn, 10.0. Found (%): C, 50.1; H, 4.7; N, 8.7; S, 5.2; Zn, 10.1. Λm ($\Omega^{-1}mol^{-1}cm^2$) = 3; FT-IR (ν, cm^{-1}): 3435, 1,642, 1,538, 1,429, 1,376, 1,217, 1,139, 500, 438.UV–Vis (λmax, nm): 260, 320, 425,**^{1}HNMR:** CH=N δ9.09 (s, 1H),OH δ9.65(s,1H disappeared with D_2O), NH δ5.96(s,1H), CH_3 δ2.51 (d 6H), CH_3COO δ3.44(s, 6H), Pyrimidin protonδ 6.68(s,2H), Aromatic protons δ6.96–8.10 (m, 10H**).**

2.5.7 | [cu (L^4)(OAc)].3H_2O

Yield 96.3%; m.p. >300 °C; green solid. Anal. Calc. for $C_{24}H_{26}N_4SO_7Cu$ (%): C, 48.5; H, 3.3; N, 9.4; S, 5.3; Cu, 10.6. Found (%): C, 52. 4; H, 4.2; N, 9.5; S, 53; Cu, 10.4.

Λm ($\Omega^{-1}mol^{-1}cm^2$) = 3; FT-IR (ν, cm^{-1}): 3445, 1,654, 1,537, 1,431, 1,396, 1,253, 1,138, 565,462.UV–Vis (λmax, nm): 260, 320, 420, 690.ESR: g_1 = 2.06, g_2 = 2.09, g_3 = 2.27; R_r = 0.85; <g> = 2.14.

2.5.8 | [Zn (HL^4)$(OAc)_2$].2H_2O

Yield 92.2%; m.p. >300 °C; orange solid. Anal. Calc. for $C_{26}H_{28}N_4SO_9Zn$ (%): C, 49.0; H, 4.2; N, 8.7; S, 5.0; Zn, 10.5. Found (%): C, 49.3; H, 4.6; N, 9.0; S, 4.9; Zn, 10.3. Λm ($\Omega^{-1}mol^{-1}cm^2$) = 3; FT-IR (ν, cm^{-1}): 3437, 1,630, 1,539, 1,428,1,380, 1,252,1,134,586, 439.UV–Vis (λmax, nm): 260, 320, 425,**^{1}HNMR:** CH=N δ9.09 (s, 1H),OH δ9.65(s,1H disappeared withD_2O), (NH) δ5.96(s,1H), (CH_3) δ2.49 (d 3H), CH_3COO δ3.44(s, 6H),Pyrimidin protonδ 6.58(s,2H),Aromatic protons δ6.71–8.13 (m, 10H**).**

2.5.9 | [cu (L^5) (OAc)].2H_2O

Yield 92%; m.p. 290 °C; green solid. Anal. Calc. for $C_{23}H_{22}N_4SO_7Cu$ (%): C, 49.1; H, 3.9; N, 9.9; S, 5.6; Cu, 11.3. Found (%): C, 49.4; H, 4.2; N, 10.3; S, 5.4; Cu, 11.3. Λm ($\Omega^{-1}mol^{-1}cm^2$) = 3; FT-IR (ν, cm^{-1}): 3443, 1,620, 1,539, 1,491, 1,339,1,277, 1,135, 570, 463. UV–Vis (λmax, nm): 270, 335, 420, 690.ESR: g = 2.12.

2.5.10 | [Zn (L^5)$_2$]

Yield 97%; m.p. 289 °C; yellow solid. Anal. Calc. for $C_{42}H_{30}N_8S_2O_6Zn$ (%): C, 57.8; H, 3.4; N, 12.8; S, 7.3; Zn, 7.5. Found (%): C, 57.6; H, 3.7; N, 12.6; S, 7.5; Zn, 7.7. Λm ($\Omega^{-1}mol^{-1}cm^2$) = 3; FT-IR (ν, cm^{-1}): 3438, 1,537, 1,336, 1,285, 1,154, 573, 438. UV–Vis (λmax, nm): 270, 340, 430, ^{1}HNMR: CH=N δ9.22 (s, 1H), (NH) δ5.97(s,1H),, Pyrimidin protonδ 6.52(d,3H),Aromatic protons δ6.55–8.45 (m, 10H).

2.6 | Computational methodology

Gas-phase geometries of **HL^1-HL^5** were optimized by DFT/B3LYP method[16] combined with 6–31 + G (d) basis set[17] using the Gaussian 03 package.[18] The optimized geometries were verified by performing frequency calculations. Full geometry optimization was performed to generate the optimized structures and ground-state properties of the studied compounds. The electronic transition properties, which include maximum excitation wavelength (λmax) and relative intensities (oscillator strengths, f), were obtained using the Time-Dependent Density Functional Theory (TD-DFT) at the same level of the theory.

2.7 | Antimicrobial activity

The ligands **HL^1-HL^5** and their copper and zinc complexes were screened *in-vitro* against pathogenic bacteria strains: (i) Gram-positive bacteria: *Streptococcus pneumonia (ATCC 49619)* and *Bacillus subtilis (ATCC6633),* (ii) Gram-negative bacteria: *Escherichia coli* (*ATCC 6538*) and *Pseudomonas aeruginosa (ATCC 9027)* and (iii) Fungi: *Candida albicans (ATCC 10231)* and *Aspergillus fumigatus (ATCC 46645). Ampicillin* and *Gentamicin* were used as standard *bacteriocide* while *Amphotericin B as* a *standard fungicide.*

The antimicrobial activity of the samples was determined using the diffusion agar method.[14] All the prepared compounds were dissolved to synthesize a stock solution of 5 mg/mL in DMSO. The solution was two-fold diluted to have solutions of various concentrations. Measuring the diameters of the inhibition zone (mm) was used to determine the antimicrobial activities. Media with DMSO was served as control.

All cultures were usually maintained on NA (nutrient agar) and incubated at 37 °C. The inoculums of bacteria were performed by growing the culture in NA broth at 37 °C for 24 h. Approximately, 0.1 mL of diluted bacterial or fungal culture suspension was spread with the help of spreader on NA plates uniformly. Solutions of the tested compounds and reference drugs were prepared by dissolving 10 mg of the compound in 10 mL DMF. A 100 mL sample was pipetted into a hole (depth 3 mm) made in the center of the agar. Sterile 8 mm discs (Hi media Pvt. Ltd.) was impregnated with test compounds. The disc was placed onto the plate and each plate had one control disc impregnated with solvent. The incubation of the plates was carried out at 37 °C for 18–48 h. Standard discs of Gentamicin and Ampicillin (Antibacterial agents were; 10 mg/disc) and Amphotericin B (Antifungal agent; 10 mg/disc) were acted as positive controls for antimicrobial activity while filter discs impregnated with 10 μL of solvent dimethyl sulfoxide were served as a negative control.

2.8 | In vitro cytotoxicity screening

The antitumor studies of **HL^1**, [Cu(**L^2**)(OAc)] and [Cu(**L^3**)(OAc)] were estimated versus three human tumors; liver cancer (HEPG2), breast cancer (MCF7) and colon cancer (HCT 116). Different concentrations of the

selected candidates were applied to determine IC_{50} values using doxorubicin as a standard. The human cell lines: Liver carcinoma cell lines (HEPG2), Breast carcinoma cell line (MCF7) and Colon carcinoma cell line (HCT 116) were achieved from VACSERA Tissue Culture Unit. Chemicals Used: Dimethyl sulfoxide (DMSO), crystal violet and trypan blue dye were procured from sigma (ST. Lous, Mo., USA). Fetal bovine serum, DMEM, RPMI-1640, HEPES buffer solution, L-glutamine, gentamycin and 0.25% Trypsin – EDTA were purchased from Lonza. Crystal violet stain (1.0%) was prepared from 0.5% (*w*/*v*) crystal violet and 50% ethanol, diluted with distilled water then filtered through a Whatman filter paper No.1. Cell lines propagation: The cell was propagated in Dulbecco's modified Eagle's medium (DMEM) supplemented with 10% heat- inactivated fetal bovine serum, 1.0% L-glutamine, HEPES buffer and 50 μg/mL gentamycin. The cells were kept at 37 °C in a humidified atmosphere with 5.0% CO_2 and were subcultured two times a week. Cell toxicity was monitored by determining the effect of the test samples on cell morphology and cell viability. Cytotoxicity evaluation using viability assay: for cytotoxicity assay, the cells were seeded in 96-well plate at a cell concentration of $1x10^4$ cells per well in 100 μL of growth medium. Fresh medium containing different concentrations of the test sample was added after 24 h of seeding. Serial two-fold dilutions of the tested chemical compound were added to confluent cell monolayers dispensed into 96-well, flat-bottomed microliter plates (Falcon, Nu, USA) using a multichannel pipette. The microliter plates were incubated at 37 °C in a humidified incubator with 5.0% CO_2 for a period of 48 h. Three wells were used for each concentration of the test samples. Control cells were incubated without a test sample and with or without DMSO. The little percentage of DMSO present in the wells (maximal 0.1) does not affect the experiment. After incubation of the cells for 24 h at 37 °C, the various concentration of the sample (50, 25, 12.5, 6.25, 3.12 and 1.56 μg) was added and the incubation was continued for 48 h and viable cells were determined by a colorimetric method. In brief, after the end of the incubation period, media were aspirated and the crystal violet solution (1.0%) was added to each well for at least 30 min. The stain was removed, and the plates were rinsed using tap water until all excess stain is removed. Glacial acetic acid (30%) was then added to all wells and mixed thoroughly, and then the absorbance of the plates was measured after gently shaken on a Microplate reader (TECAN, Inc.), using a test wavelength of 490 nm. All results were corrected for background absorbance detected in wells without added stain. Treated samples were compared with the cell control in the absence of the tested compounds. All experiments were carried out in triplicate. The cell cytotoxic effect of each tested compound was calculated.[15,19] The inhibitory activity IC_{50} of Doxorubicin, the standard drug versus the studied carcinoma cell lines was identified under the above studied environments.

3 | RESULTS AND DISCUSSIONS

3.1 | Synthesis and characterization

The targeted nanosized organic ligands, **HL^1-HL^5** were prepared by the nanoprecipitation reaction, Scheme 1, of equimolar ratios of the aldehyde and the sulfonamide drug namely; sulfamethazine, sulfamerazine or sulfadiazine in a mixture of dioxane/H_2O (10: 1, *V*/V) under ultrasonic conditions at 42 kHz for 1 h..

Interestingly, the desired particles were obtained as well-separated spherical morphology, Figure 2, with some interconnection degree. The tendency of spherical particle formation of the prepared sulfonamide imine derivatives could be related to the distribution stability of particles in the reaction medium or the precipitation mechanism of the particles.[20] The average diameter of the particles calculated from SEM images based on numerous particles selected randomly, ranges from 44–150 nm and the association between particles was present in a larger or smaller extent. The average diameters of sulfonamide imine ligands prepared from sulfamethazine **HL^1** and **HL^3** were 70 nm and 100 nm; standard deviations were 5.85 and 11.69, respectively. The average diameter nanosized sulfonamide imine ligands prepared from sulfamerazine drug exhibited a small average diameter compared to their sulfamethazine counterpart. The average diameters for **HL^2** and **HL^4** are 56 nm and 44 nm; standard deviations are 13.60 and 7.44, respectively. Based on the obtained results, the presence of two methyl substituents on the pyrimidine ring increased the ligand nanosized.[21,22]

The heating ethanolic solution of hydrated metal acetate (copper or zinc) with an equimolar ratio of the appropriate organic ligands **HL^1–HL^5** furnished the corresponding complexes and their melting points are in the range of 219–300 °C. The non-electrolytic nature of the prepared metal complexes was concluded from their lower molar conductivity values.

3.1.1 | Geometry optimization and time-dependent density functional theory (TD-DFT) of the organic compounds

The fully optimized geometries of the investigated ligands **HL^1-HL^5** where the numbers of atoms are presented in

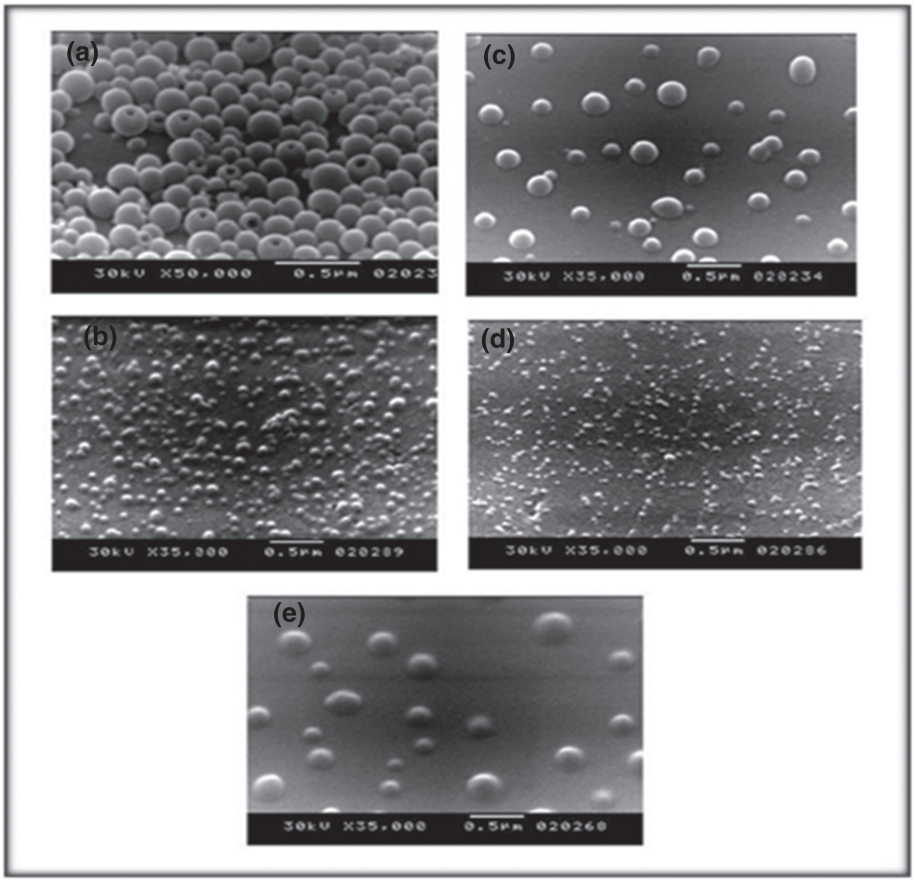

FIGURE 2 SEM images of the nanosized sulfonamide imine ligands: (a) **HL^1**, (b) **HL^2**, (c) **HL^3**, (d) **HL^4**, (e) **HL^5**

Figure 3 and their selected geometric parameters bond lengths, bond angles and dihedral angles are listed in Table 1. The optimized geometries of the investigated sulfonamide imine compounds suggest that the C-C, C-O, C-N, S=O and S-N bond distances were found to be in the range 1.346–1.462, 1.346–1.351, 1.301–1.424, ° and the dihedral angles are in the range −119-156°, respectively. The bond angles were found to be in the range 97–125 °1.437–1.438 and 1.755–1.760 A

The HOMO represents the electron-donating ability of the molecule to donate electrons to appropriated acceptor molecules with low-energy, empty molecular orbital. The lower value of LUMO indicates the high ability of the molecule to accept electrons.[23] While, the higher value of HOMO of the ligand, the easier is its ability to offer electrons. Furthermore, the smaller value of the HOMO-LUMO energy gap, ΔE, the lower stability and higher reactivity of the compound.[23] The optimized geometry of the studied molecules, molecular frontier orbitals, HOMO and LUMO, are visualized with Gaussian view.[24,25] The charge density distribution, HOMO and LUMO, for the free ligands **HL^1-HL^5** are presented in Figure 4. The dipole moment μ calculated from the first derivative of the energy to an applied electric field, was used to discuss and rationalize the structure. Quantum chemical parameters of the ligands **HL^1-HL^5** were obtained from the calculations including the energies of the HOMO and the LUMO, absolute electronegativities, χ, chemical potentials, Pi, absolute hardness, η, absolute softness, σ, global electrophilicity, ω, global softness, S, and additional electronic charge, ΔNmax, were calculated using the following equations (1–8) and listed in Table 2.

$$\Delta E = E_{LUMO} - E_{HOMO} \quad (1)$$

$$\chi = -\frac{(ELUMO + EHOMO)}{2} \quad (2)$$

$$\eta = \frac{ELUMO - EHOMO}{2} \quad (3)$$

$$\sigma = \frac{1}{\eta} \quad (4)$$

$$Pi = -\chi \quad (5)$$

$$S = \frac{1}{2\eta} \quad (6)$$

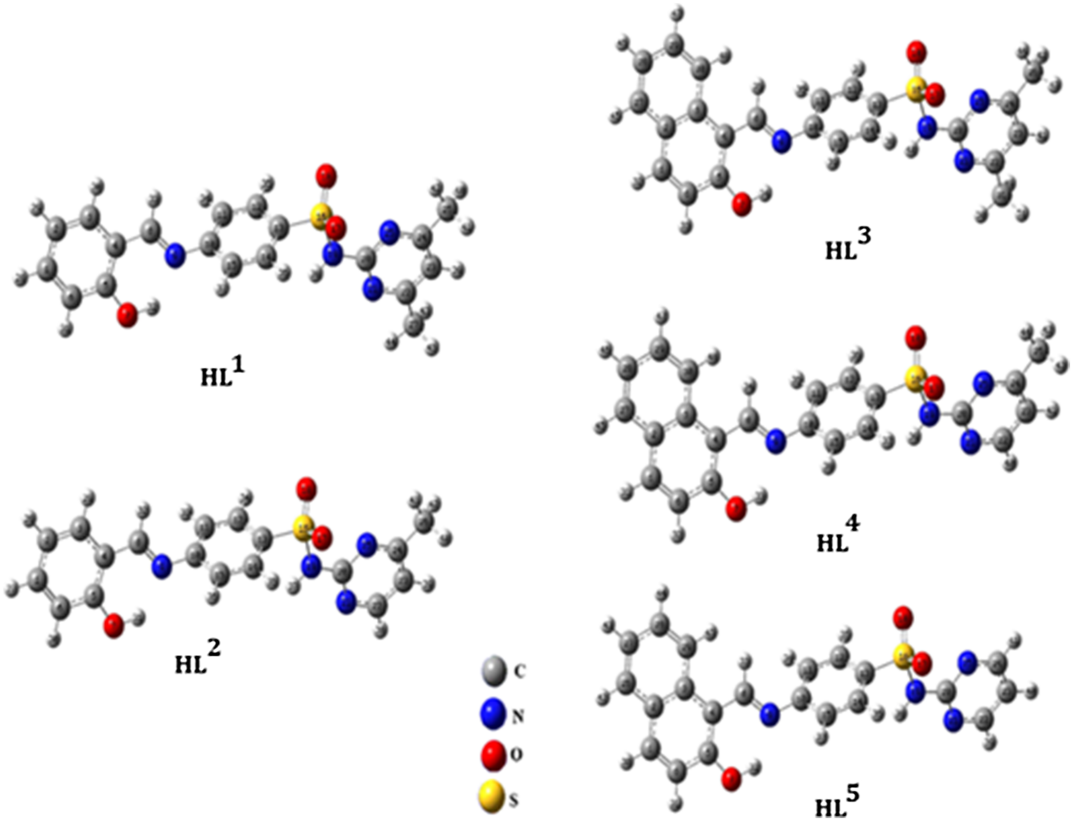

FIGURE 3 The fully optimized geometries of the investigated ligands $\mathbf{HL^1}$ $\mathbf{HL^5}$ and numbering of atoms by DFT/B3LYP method

$$\omega = \frac{Pi^2}{2\eta} \tag{7}$$

$$\Delta \mathrm{Nmax} = -\frac{Pi}{\eta} \tag{8}$$

An inspection of the results reveals that the value of ΔE for $\mathbf{HL^1}$**and** $\mathbf{HL^2}$ ligands are found to be 0.1517 eV and 0.1552 eV, respectively, indicating that the $\mathbf{HL^1}$ ligand is less stable and more reactive than $\mathbf{HL^2}$ ligand. This is quite reasonable where the presence of the two-CH_3 groups (electron-donating group) on the pyrimidine moiety will enhance the electron density by their positive inductive effect, revealing the co-planarity of the molecule and thus affording a maximum resonance via delocalization π-system. However, the value of ΔE for $\mathbf{HL^3}$– $\mathbf{HL^5}$ ligands increases in the order $\mathbf{HL^3} > \mathbf{HL^4} > \mathbf{HL^5}$, leading to the opposite effect. Additionally, the higher HOMO energy value of $\mathbf{HL^5}$ compared to $\mathbf{HL^3}$and $\mathbf{HL^4}$ indicated its high ability to offer electrons and its lower LUMO energy value indicated its high ability to accept electrons.[23]

To gain detailed insight into the charge transitions, the theoretical electronic spectra were calculated by using time-dependent density functional theory (TD-DFT) method. Frontier molecular orbitals (FMO) were performed at the same level of theory. The theoretical absorption spectra were simulated using Gaussian software. TD-DFT results and the calculated excitation wavelengths of the investigated $\mathbf{HL^5}$ free ligands and their assignments are displayed in Table 3. and TDDFT-calculated electronic transitions in sulfonamide imine ligands $\mathbf{HL^1}$and $\mathbf{HL^3}$ are displayed in Figures 5 and 6 as representative examples.

The TD-DFT studies for the sulfonamide imine ligand, 4-{[(1E)-(2-hydroxy-1-salicyl) methylene] amino}-N-(4, 6)- dimethyl pyrimidine- 2-yl) benzene sulfonamide, ($\mathbf{HL^1}$), **(**Figure 5) and Table 4, represent six main absorption bands at 663.67, 589.81, 469.88, 464.92, 393.00 and 390.31 nm. The calculated band at 663.67 nm arises from the transitions of π electrons from HOMO to LUMO/LUMO+4 as relative to π (py) - π *(saly/Azo-m/An)/π *(saly). The broad calculated band at 589.81 nm arises from the transitions of [π (an)- π *(An), π (saly/Azo-m/An)- π *(saly/An) and π (py)- π *(saly/An)]from HOMO/HOMO-2/HOMO-5 to LUMO +1/LUMO+2; the calculated band at 469.88 nm arises from the transitions of π electrons from HOMO-1to LUMO+6 which represents π (py)- π *(py) transition. The broad calculated band at 464.92 nm arises from the transitions of π electrons from HOMO/HOMO-4 to

TABLE 1 Selected calculated bond lengths (A°), bond angles (°) and dihedral angles(°) for sulfonamide imine ligands

	Sulfonamide imine ligands				
Bond length (A°)	**HL^1**	**HL^2**	**HL^3**	**HL^4**	**HL^5**
C(3)-C(4)	1.418	1.418	1.447	1.447	1.447
C(4)-C(5)	1.414	1.414	1.400	1.400	1.400
C(4)-C(8)	1.462	1.461	1.456	1.456	1.455
C(5)-O(7)	1.351	1.351	1.346	1.346	1.346
C(8)-N(9)	1.301	1.301	1.306	1.306	1.306
N(9)-C(10)	1.424	1.423	1.423	1.423	1.422
S(16)-O(17)	1.438	1.438	1.438	1.438	1.437
S(16)-O(18)	1.438	1.438	1.438	1.438	1.437
S(16)-N(19)	1.755	1.757	1.756	1.756	1.760
N(19)-C(20)	1.394	1.393	1.394	1.394	1.392
C(20)-N(21)	1.383	1.385	1.383	1.383	1.386
Bond Angle (°)	**HL^1**	**HL^2**	**HL^3**	**HL^4**	**HL^5**
C(8)-N(9)-C(10)	123.91	123.970	123.590	123.627	123.665
C(4)-C(5)-O(7)	125.029	125.040	125.474	125.483	125.487
C(4)-C(8)-N-(9)	120.351	120.368	120.334	120.351	120.369
C(13)-S(16)-O(17)	108.756	108.885	108.825	108.954	109.087
C(13)-S(16)-O(18)	108.630	108.759	108.667	108.797	108.928
C(13)-S(16)-N(19)	97.015	97.068	97.008	97.061	97.112
S(16)-N(19)-C(20)	121.644	121.673	121.679	121.717	121.911
N(19)-C(20)-N(21)	118.414	118.589	118.405	118.581	118.461
Dihedral angle(°)	**HL^1**	**HL^2**	**HL^3**	**HL^4**	**HL^5**
C(8) -N(9) -C(10) -C(11)	−66.433	−66.908	−57.621	−57.707	−58.014
C(13) -S(16)-O(18)- C(12)	21.347	21.288	21.352	21.277	20.991
-C(13) -S(16) -O(17) C(12)	156.371	156.523	156.433	156.573	156.764
C(13) -S(16) -N(19) -C(12)	−91.117	−91.073	−91.076	−91.043	−91.093
C(23)- C(24) -C(26) -H40)	60.114	−60.353	----------	--------	-------
C(23) -C(24)- C(26)- H(41)	−60.353	----------	---------	-------	-------
C(23)- C(24)-C(26)- H(42)	----------	60.142	60.065	60.071	------
C(21)- C(22)- C(27)-H(43)	120.175	---------	−60.450	−60.427	-------
C(21)- C(22)- C(27)-H(45)	−119.861	----------	---------	---------	------
C(21)- C(22)-C(31)- H(49)	---------	----------	119.995	--------	------
C(21)- C(22)- C(31)- H(51)	---------	---------	−120.041	-------	------

1.437-1.438 and 1.755-1.760 A°, respectively. The bond angles were found to be in the range 97-125 ° and the dihedral angles are in the range -119-156°.

LUMO+4 [π (saly/Azo-m/An) or π (py)- π *(saly). The highest energy broad calculated band at 393.00 nm arises from the transitions of π electrons from HOMO/HOMO- 2 to LUMO/LUMO+7 [π (saly/Azo-m/An)- π *(saly/Azo-m/An) and π (py)- π *(saly/Azo-m)],the broad calculated band at 390.31 nm arises from transitions of π electrons from HOMO/HOMO-4 to LUMO which refers to [π (saly/Azo-m/An) or π (py)-π *(saly/Azo-m/An)].

The TD-DFT studies of the free ligand (4-{[(1E)-(2-hydroxy-1-naphthyl) methylene] amino}-N-(4, 6)-dimethyl pyrimidine- 2-yl) benzene sulfonamide) **HL^3**, ligand Figure 6 and Table 3, imply six main absorption bands at 797.51, 597.32, 548.90, 469.86, 422.22 and 411.12 nm. The calculated band at 797.51 nm arising from transitions of π electrons corresponds from HOMO to LUMO as relative to π (naph)- π *(naph/Azo-m/An). The calculated band at 597.32 nm arises from transitions

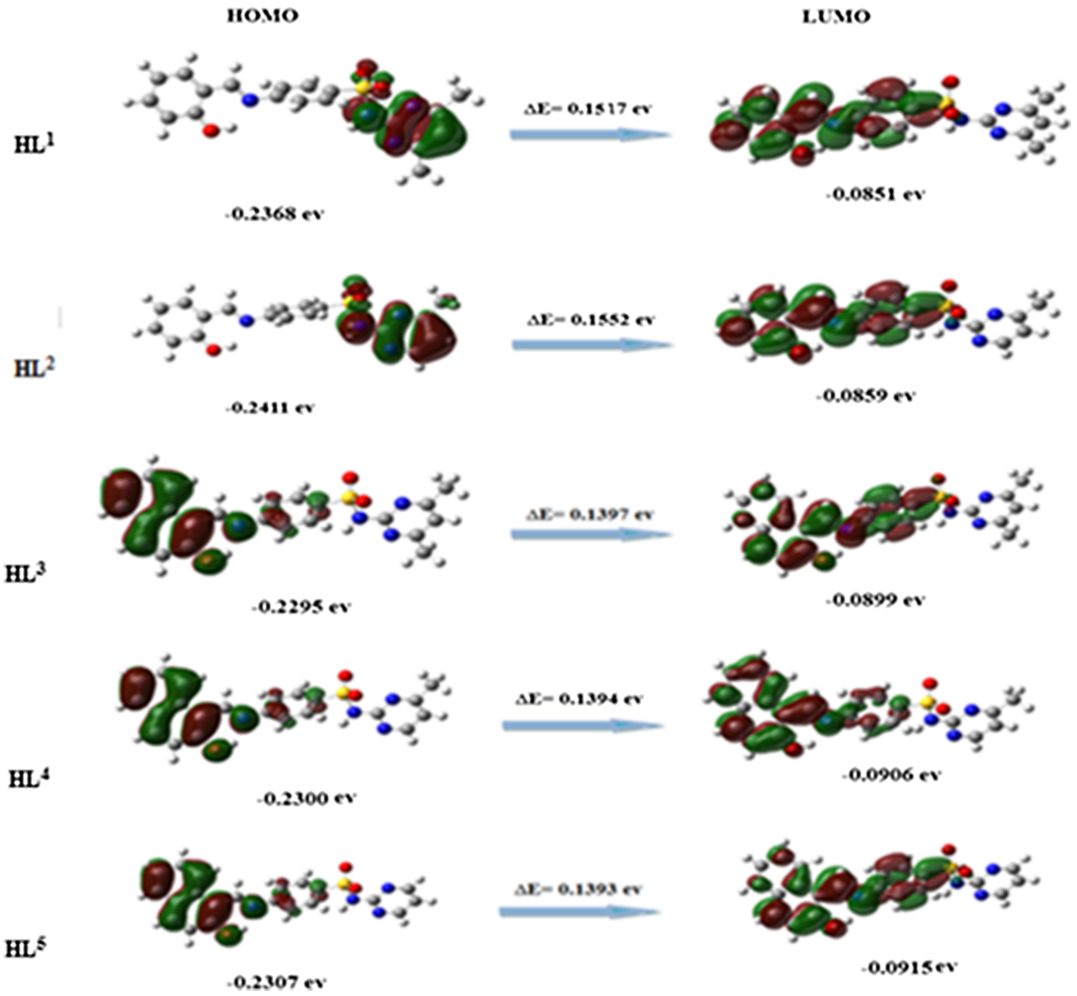

FIGURE 4 Molecular frontier orbitals HOMO and LUMO of sulfonamide imine ligands **HL^1-HL^5**

TABLE 2 The calculated quantum chemical parameters for sulfonamide imine compounds HL^1-HL^5

Molecule	E_{HOMO} (eV)	E_{LUMO} (eV)	ΔE (eV)	μ (D)	E tot (AU)	X (eV)	ŋ (eV)	σ (eV)$^{-1}$	Pi (eV)	S (eV)$^{-1}$	ω (eV)	ΔN max
HL^1	−0.2368	−0.0851	0.1517	3.436	− 1577.705	0.1609	0.0759	13.184	−0.161	6.591	0.171	2.121
HL^2	−0.2411	−0.0859	0.1552	3.454	− 1538.383	0.1635	0.0776	12.886	−0.163	6.443	0.171	2.101
HL^3	−0.2295	−0.0899	0.1396	3.991	− 1731.349	0.1597	0.0698	14.326	−0.160	7.163	0.183	2.292
HL^4	−0.2300	−0.0906	0.1394	4.023	− 1692.026	0.1603	0.0697	14.347	−0.160	7.174	0.184	2.295
HL^5	−0.2307	−0.0915	0.1393	4.740	− 1652.703	0.1611	0.0696	14.367	−0.161	7.179	0.186	2.313

from HOMO/HOMO-3 to LUMO+1 of [π (naph/Azo-m/An)- π *(naph/Azo-m/An)]; the calculated band at 548.90 nm arises from the transitions of π electrons from HOMO to LUMO/LUMO+6 which represent [π (naph)- π *(naph/Azo-m/An)/π *(Azo-m/An)]. The calculated band at 469.86 nm arises from transitions of π electrons from HOMO-9 to LUMO+4 [π (py) - π *(py)]. The calculated band at 422.22 nm arises from transitions of π electrons from HOMO/HOMO-2 to LUMO/LUMO+2 [π (naph/Azo-m/An) - π *(naph/Azo-m/An) and π (naph)-π *(naph)] The highest energy calculated band at 411.12 nm arises from transitions of HOMO to LUMO+8 [π (naph)- π *(naph/Azo-m)].

3.1.2 | FTIR spectra of HL^1-HL^5 and their complexes

The υ (C=N) azomethine band for **HL^1–HL^5** is located at 1595, 1594, 1,589, 1,570 and 1,581 cm^{-1}, respectively. The

TABLE 3 Calculated triplet excitation energies, wave lengths, and their contributions for the sulfonamide imine ligands

Excitation energy (eV)	Wave length (nm)	Contributions
HL^1		
1.8682	663.67	HOMO-LUMO, HOMO→LUMO+4
2.1021	589.81	HOMO-5 → LUMO+2, HOMO-2 → LUMO+1, HOMO → LUMO+1
2.6386	469.88	HOMO-1 → LUMO+6
2.6668	464.92	HOMO-4 → LUMO+4, HOMO → LUMO+4
3.1548	393.00	HOMO-2 → LUMO, HOMO → LUMO +7
3.1766	390.31	HOMO-4 → LUMO, HOMO → LUMO
HL^2		
1.8687	663.49	HOMO → LUMO, HOMO → LUMO+4
2.1027	589.64	HOMO-5 → LUMO+2, HOMO-2 → LUMO+2
2.6328	470.92	HOMO-1 → LUMO+6
2.6670	464.88	HOMO → LUMO+4
3.1552	392.95	HOMO-2 → LUMO
3.1759	390.39	HOMO-4 → LUMO, HOMO→ LUMO
HL^3		
1.5546	797.51	HOMO → LUMO
2.0757	597.32	HOMO-3 → LUMO+1, HOMO → LUMO+1
2.2588	548.90	HOMO → LUMO, HOMO → LUMO+6
2.6388	469.86	HOMO-9 → LUMO+4
2.9365	422.22	HOMO-2 → LUMO, HOMO → LUMO +2
3.0158	411.12	HOMO → LUMO+8
HL^4		
1.5548	797.42	HOMO → LUMO
2.0763	597.13	HOMO-3 → LUMO+1, HOMO → LUMO
2.2584	548.99	HOMO → LUMO+6
2.6328	470.93	HOMO-1 → LUMO+7
2.9363	422.24	HOMO-2 → LUMO, HOMO → LUMO +2
3.0165	411.03	HOMO → LUMO+2, HOMO →LUMO +8
HL^5		
1.5549	797.36	HOMO → LUMO
2.0776	596.76	HOMO → LUMO+1
2.2579	549.12	HOMO → LUMO, HOMO → LUMO+6
2.6082	475.37	HOMO-2 → LUMO+7
2.9364	422.24	HOMO-1 → LUMO, HOMO → LUMO +3
2.9364	410.95	HOMO-1 → LUMO

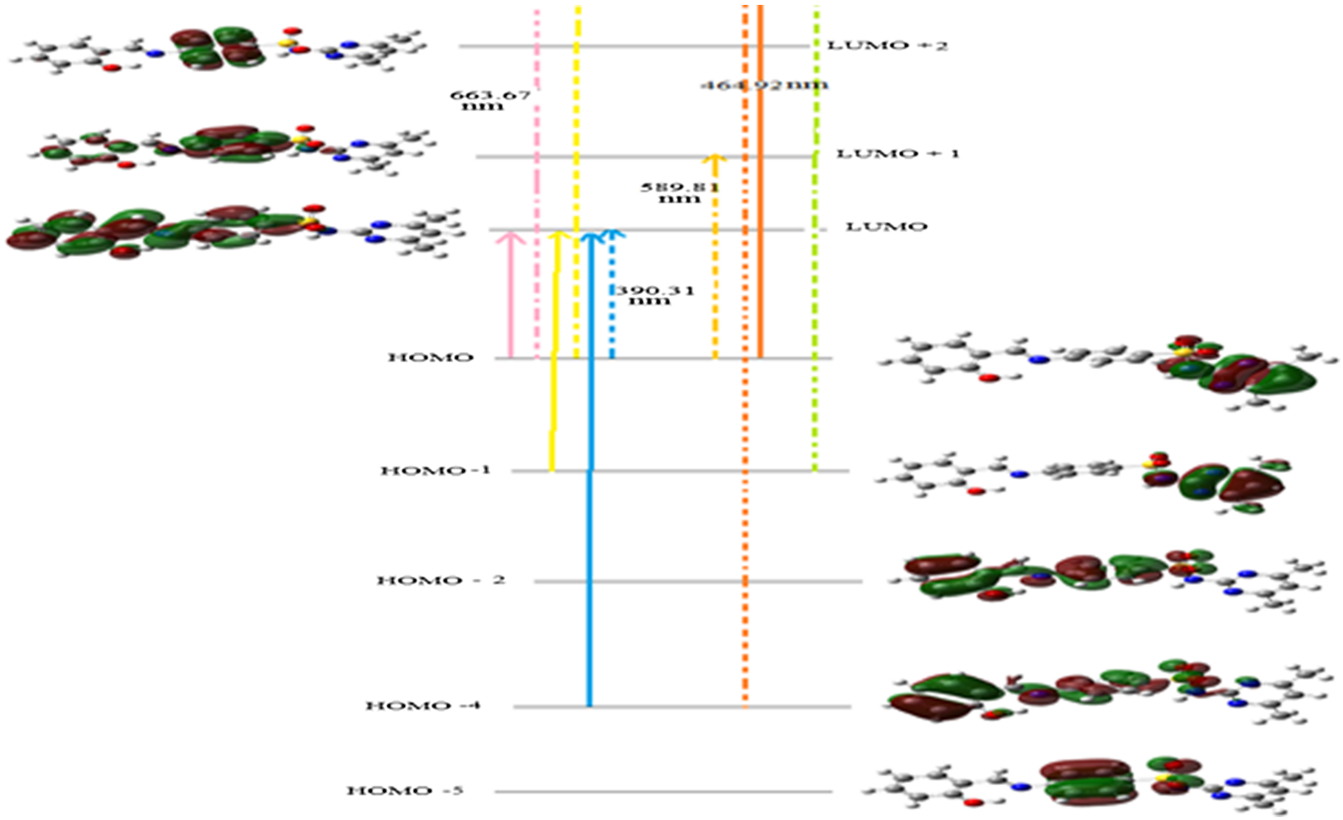

FIGURE 5 TD-DFT calculated electronic transitions in sulfonamide imine 4-{[(1E)- (2-hydroxy-1-salicyl) methylene] amino}-N-(4, 6)-dimethyl pyrimidine-2-yl) benzene sulfonamide, **(HL^1)**

difference in stretching vibration of the azomethine group may be due to the steric and/or electronic effect of the substituents on the aromatic rings. The spectra of **HL^1–HL^5** exhibit broadbands at 3393, 3436, 3,444, 3,461 and 3,456 cm^{-1}, respectively, due to υ (OH) and υ (NH) of the sulfonamide groups. The broad nature and the low-frequency position of these bands could be taken as a proof for the involvement of these two groups in intra- and/or intermolecular hydrogen bonding. The hydroxyl and the azomethine groups are oriented to form hydrogen bond of intramolecular type (O-H----N=C) forming a stable six-membered while the sulfonamide (NH) group and its adjacent -SO_2 and/or pyrimidine nitrogen are not in positions to form stable intramolecular hydrogen bonding but maybe participated in an intermolecular hydrogen bonding of the type (N-H ... O=S=O ... N-H). The FT-IR spectra of the free ligands displayed two bands at 1310–1340 cm^{-1} and 1,149–1,155 cm^{-1} due to υ $(SO_2)_{asym}$ and υ $(SO_2)_{sym}$, respectively. Furthermore, the spectra of the ligands displayed a medium-strong band in the range 1,238–1,261 cm^{-1}, due to phenolic υ(C-O) confirming the participation of the phenolic OH in H-bonding.[26] Furthermore, the ligands exhibited the pyrimidine $\upsilon_{(C=N)}$ at 1513–1567 cm^{-1} as only one strong-medium band suggesting that the two C=N groups in the pyrimidine moiety are equivalent. Generally, the FT-IR spectra of the Cu (II) and Zn (II) complexes displayed a medium-strong band at 1512–1569 cm^{-1} due to υ $(C=N)_{azomethine}$ compared to that of the ligands that found at 1570–1595 cm^{-1}. The lower shift of υ(C=N) ranging from 58 to 26 cm^{-1} on chelation indicated the coordination of the azomethine nitrogen to the metal ion.[27] The spectra of the metal (II) complexes displayed a band at 1520–1554 cm^{-1} due to υ $(C=N)_{Pyrimidine}$ similar to that of the ligands suggesting a non-bonding nature of the pyrimidine nitrogen atoms. The characteristic band of $\upsilon(C\text{-}O)_{phenolic}$ was upward shifted by 15–24 cm^{-1} in copper complexes, $[Zn(\mathbf{L^1})_2].2H_2O$ and $[Zn(\mathbf{L^5})_2]$ confirming the coordination of the deprotonated phenolic-OH, whereas no appreciable shift of this specific band was noticed in the case of $[Zn\ (\mathbf{HL^2})_2(OAc)_2]$, [Zn **($\mathbf{HL^3}$)** $(OAc)_2].2H_2O$ and [Zn **($\mathbf{HL^4}$)**$(OAc)_2].2H_2O$ indicating the bonding of the phenolic OH to the metal ion.

All copper complexes exhibited new medium bands at υ 1,607–1,656 cm^{-1} and 1,410–1,491 cm^{-1} assignable to υ_{asym} (COO^-) and υ_{sym} (COO^-), respectively. The

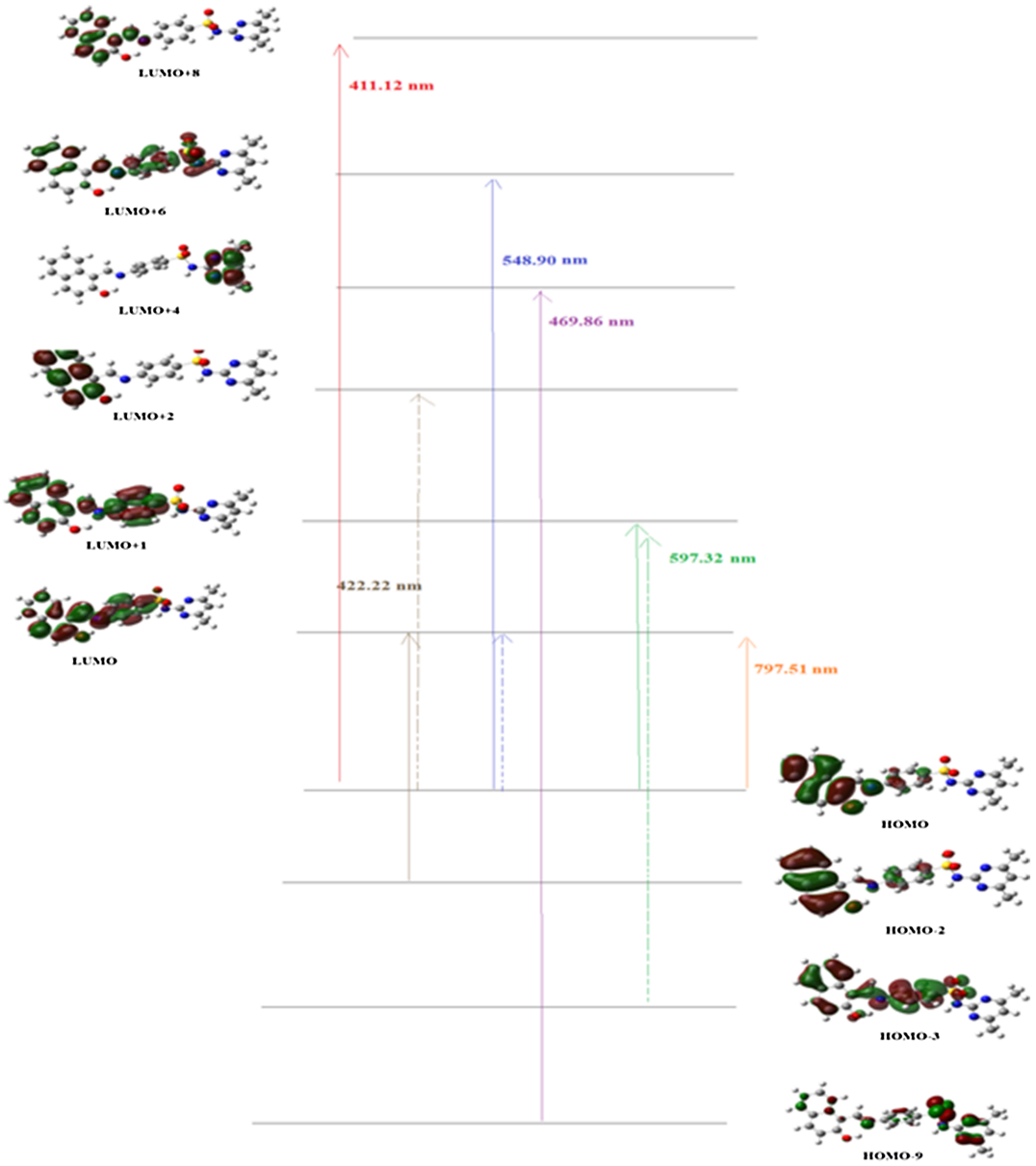

FIGURE 6 TD-DFT calculated electronic transitions in sulfonamide imine 4-{[(1E)- (2-hydroxy-1-naphthyl) methylene] amino}-N-(4, 6)- dimethyl pyrimidine- 2-yl) benzene sulfonamide, **(HL^3)**

magnitude of separation ($\Delta\upsilon = \upsilon_{asym}-\upsilon_{sym}$) is in the range of 165–197 cm^{-1} in all complexes except for [Zn **(HL^3)**$(OAc)_2$].$2H_2O$ and [Zn (HL^4)$(OAc)_2$].$2H_2O$ which suggests the bidentate coordination of the acetate group.[28] The value of $\Delta\upsilon = 202$ cm^{-1} in the case of [Zn **(HL^3)**$(OAc)_2$].$2H_2O$ and [Zn (HL^4)$(OAc)_2$].$2H_2O$ confirmed the monodentate nature of the acetate group.[28] All complexes displayed medium broad bands at 3200–3500 cm^{-1} characteristic to ν (NH) and ν (OH) and bands at 500–586 and υ 425–462 cm^{-1} related to ν (M–N) and ν (M–O), respectively, supporting the coordination to the ligands.[27]

3.1.3 | Electronic spectra

The electronic spectra of the organic ligands and their Cu (II) and Zn (II), complexes were recorded as 10^{-5} M DMSO solution in the wavelength range of 200–1,000 nm. The spectra of **HL^1–HL^5** showed high intense bands at 260–270, 320–355 and 415–475 nm due to the intra- ligand $\pi \rightarrow \pi^*$, $n \rightarrow \pi^*$ and charge transfer transitions, respectively, and rather consistent with the literature data.[29] The [Cu(**L^2**)(OAc)].nH_2O, [Cu(**L^3**)(OAc)].H_2O, [Cu(**L^4**)(OAc)].$3H_2O$, and [Cu(**L^5**)(OAc)].$2H_2O$ exhibited broad bands at λ 690–700 nm

TABLE 4 Thermal analyses of sulfonamide imine ligands and their metal (II) complexes

Compound No.	Steps	TG (°C)	DTG (°C)	Mass loss (%) Found (Calculated)	Fragment	DTA (°C)
HL [1]	I	250–457	325	24.37(24.34)	C_6H_5O	87.1(Endo.)
	II	457–800	575	75.625(75.65)	$C_{13}H_{13}SO_2N_4$	530(Exo.)
[Cu(L [1]) (OAc)]	I	80–121	80	11.73(11.71)	$C_2H_3O_2$	81.4(Endo.)
	II	121–177	150	5.43(5.36)	CHN	361.3(Exo.)
	III	177–310	260	27.82(27.80)	$C_6H_4O_2S$	
	IV	310–550	360	42.39(42.50)	$C_{12}H_{12}ON_3$	
		Residue		12.60(12.61)	Cu	---
[Zn (L [1]) 2].2H 2 O	I	80–144	90	4.17(4.16)	$2H_2O$	94.7(Endo.)
	II	144–344	224	42.33(42.27)	$C_{19}H_{17}O_2SN_4$	463and572.2(Exo)
	III	344–580	570	44.07(44.12)	$C_{19}H_{17}O_3SN_4$	
		Residue		9.41(9.42)	ZnO	---
HL [2]	I	80–300	85	25.25(25.27)	C_6H_5O	89.7(Endo.)
	II	300–650	305and550	74.74(74.72)	$C_{12}H_{11}O_2N_4S$	527.1(Exo.)
[Cu (L [2])(OAc)]	I	80–120	85	12.05(12.05)	$C_2H_3O_2$	84(Endo.)
	I	120–185	135	5.52(5.51)	CHN	476(Exo.)
	III	185–280	230	28.63(28.06)	$C_6H_4O_2S$	
	IV	280–490	340and470	40.87(40.85)	$C_{11}H_{10}ON_3$	
		Residue		12.91(12.97)	Cu	---
[Zn (HL [2]) 2 (OAc) 2]	I	84–260	150	11.11(10.87)	$C_4H_6O_3$	84(Endo.)
	II	260–505	425	40.02(40.02)	$C_{18}H_{16}O_3SN_4$	427.3(Exo.)
	III	505–670	560	40.06(40.02)	$C_{18}H_{16}O_3SN_4$	560.6(Exo.)
		Residue		8.79(8.85)	ZnO	---
HL [3]	I	220–370	295	35.89(35.87)	$C_6H_5O_2SN$	103.2(Endo.)
	II	370–454	416	6.32(6.25)	CHN	540.1(Exo.)
	III	454–765	570	57.77(57.87)	$C_{22}H_{18}ON_2$	
[Cu (L [3])(OAc)]	I	80–217	150	10.69(10.65)	$C_2H_3O_2$	112.9(Endo.)
	II	217–397	340	30.59(30.53)	$C_{11}H_7NO$	473.3(Exo.)
	III	397–572	478	47.18(47.33)	$C_{12}H_{12}O_2N_3S$	
		Residue		11.52(11.47)	Cu	---
[Zn (HL [3])(OAc) 2].2H 2 O	I	80–115	85	5.55(5.52)	$2H_2O$	86.1(Endo.)
	II	115–360	250	15.68(15.65)	$C_4H_6O_3$	568.6(Exo.)
	III	360–640	425and590	66.25(66.31)	$C_{23}H_{20}N_4SO_3$	
	IV	Residue		12.51(12.49)	ZnO	---
HL [4]	I	135–419	295	36.98(37.08)	$C_6H_5O_2SN$	94.9(Endo.)
	II	419–755	575	63.01(62.91)	$C_{16}H_{13}ON_3$	568.9(Exo.)
[Cu (L [4])(OAc)].3H 2 O	I	80–155	150	19.12(19.03)	$C_2H_9O_5$	82.6(Endo.)
	II	155–295	230	23.94(23.92)	$C_{10}H_6O$	311.9(Exo.)
	III	295–487	305and435	46.22(46.67)	$C_{12}H_{11}N_4SO$	
		Residue		10.70(10.69)	Cu	---
[Zn (HL [4])(OAc) 2].2H 2 O	I	80–100	85	5.677(5.64)	$2H_2O$	82.3(Endo.)
	II	100–210	165	16.03(16.00)	$C_4H_6O_3$	558.6(Exo.)
	III	210–647	340,456and555	65.52(65.57)	$C_{22}H_{18}N_4SO_3$	

(Continues)

TABLE 4 (Continued)

Compound No.	Steps	TG (°C)	DTG (°C)	Mass loss (%) Found (Calculated)	Fragment	DTA (°C)
		Residue		12.77(12.77)	ZnO	---
HL ^{5}	I	180–430	320	38.33(38.36)	$C_6H_5O_2SN$	117.4(Endo.)
	II	430–763	560	61.44(61.63)	$C_{15}H_{11}ON_3$	544.9(Exo.)
[Cu(L ^{5} **)(OAc)].2H** $_{2}$ **O**	I	80–176	95	16.96(16.91)	$C_2H_7O_4$	81.6(Endo.)
	II	176–410	312	25.32(25.28)	$C_{10}H_6O$	489.7(Exo.)
	III	410–650	490	46.39(46.48)	$C_{11}H_9O_2N_4S$	
		Residue		11.31(11.30)	Cu	---
[Zn (L ^{5} **)** $_{2}$ **]**	I	79–260	165	44.41(44.41)	$C_{20}H_{14}O_3N_3S$	79.7(Endo.)
	II	260–644	330and590	46.27(46.24)	$C_{20}H_{14}O_4N_3S$	589.3(Exo.)
		Residue		9.31(9.34)	ZnO	---

referred to $^{2}B_{1g} \rightarrow {}^{2}B_{2g}$ transition corresponding to a tetragonally distorted copper (II) complexes ion.[30,31] The spectrum of [Cu(**L**^{1})(OAc)] showed solely a single broadband at 765 nm consistent with tetragonally distorted or trigonal bipyramidal copper geometry.[30] The UV–Vis spectra of zinc complexes did not exhibit a d-d transitional band characteristic of d^{10} species. Furthermore, their spectral bands are nearly similar to their precursor ligands with red or blue shifts. According to the empirical formula supported by other data such as elemental analysis and spectroscopic data, a tetrahedral geometry for all Zn (II) complexes was proposed, except [Zn (**HL**^{2})$_2$(OAc)$_2$] complex where octahedral geometry was estimated.

3.1.4 | ^{1}H NMR spectra of the ligands and their Zn (II) complexes

The ^{1}H-NMR spectra of the sulfonamide imines **HL**^{1}-**HL**^{5} were performed in DMSO-d6. The ^{1}H-NMR spectrum of **HL**^{1}, is given in the supporting information (Figure S1), was selected as a representative example. Four isomers in (8:5:2:1) ratio were easily identified by the presence of four CH_3 protons signals according to their relative abundance at δ 2.23 ppm, 2.20 ppm, 2.28 ppm and 2.26 ppm, respectively. The singlet signal of the azomethine proton of the isomeric mixture resonated at δ 8.93 ppm, δ 8.90 ppm, δ 8.89 ppm while that belongs to the minor isomer could be buried under other signals. The deuteratable broad singlet signal at δ 5.21 ppm was attributed to the NH proton. The aromatic protons appeared subsequently as multiplet signals. The presence of such isomers was attributed to enolimine-ketoamine tautomerism by intramolecular proton transfer. It has been reported that in a highly polar solvent as DMSO, the enolic tautomer could be present in more than one form.[32] The enol tautomer could be observed as a resonance hybrid of two canonical structures, the quinoid and/or zwitterionic forms, Figure 7. In general, polar solvents shifted the enol-keto equilibrium towards the enolic form.[33,34] The solvent protonates the imino bond-forming several possible intermediates including a zwitterionic form which favor molecular polarity and thus, the electrostatic intermolecular interactions become stronger. The keto-amine tautomer could be either *cis* or *trans* relative to the C=N bond.[35]

The ^{1}H-NMR spectra of the prepared organic ligands **HL**^{2} **HL**^{5} showed broad singlet signal at δ11.77-δ11.82 ppm corresponding to the deuteratable OH. The two singlet signals at δ10.14 and 10.13 ppm in the spectrum of **HL**^{2} and δ9.65 and 9.64 ppm in the spectrum of **HL**^{3} corresponded to azomethine proton. However, the HC=N proton appeared at δ 9.57 and 9.59 ppm in the spectrum of **HL**^{4} and **HL**^{5} respectively. The aromatic protons resonated at δ 8.86–6.55 ppm. The spectrum of **HL**^{2} exhibited methyl protons at δ2.27 (s, 3H, major) and δ 2.29 (s, 3H, minor). In a similar fashion, the spectrum of **HL**^{3} displayed a singlet at δ δ 2.23 (s, 3H, major) and δ 2.20 (s, 3H, CH_3, minor) assignable to methyl protons. Analogously the ^{1}H-NMR spectrum of **HL**^{4} recorded a methyl signal at δ 2.32 (s, 3H, CH_3).

Zinc (II) complexes exhibited similar singlet at δ 10.05–8.60 ppm, assigned to azomethine (-CH=N) proton. This specific proton resonated relatively at a lower field than that of the ligand (Δδ = +1.07 to 0.27 ppm) indicating azomethine's nitrogen-Zn (II) coordination. The absence of phenolic-OH signal in the case of [Zn(L^{1})$_2$].2H$_2$O and [Zn(L^{5})$_2$] confirmed its deprotonation upon complexation. The spectra of

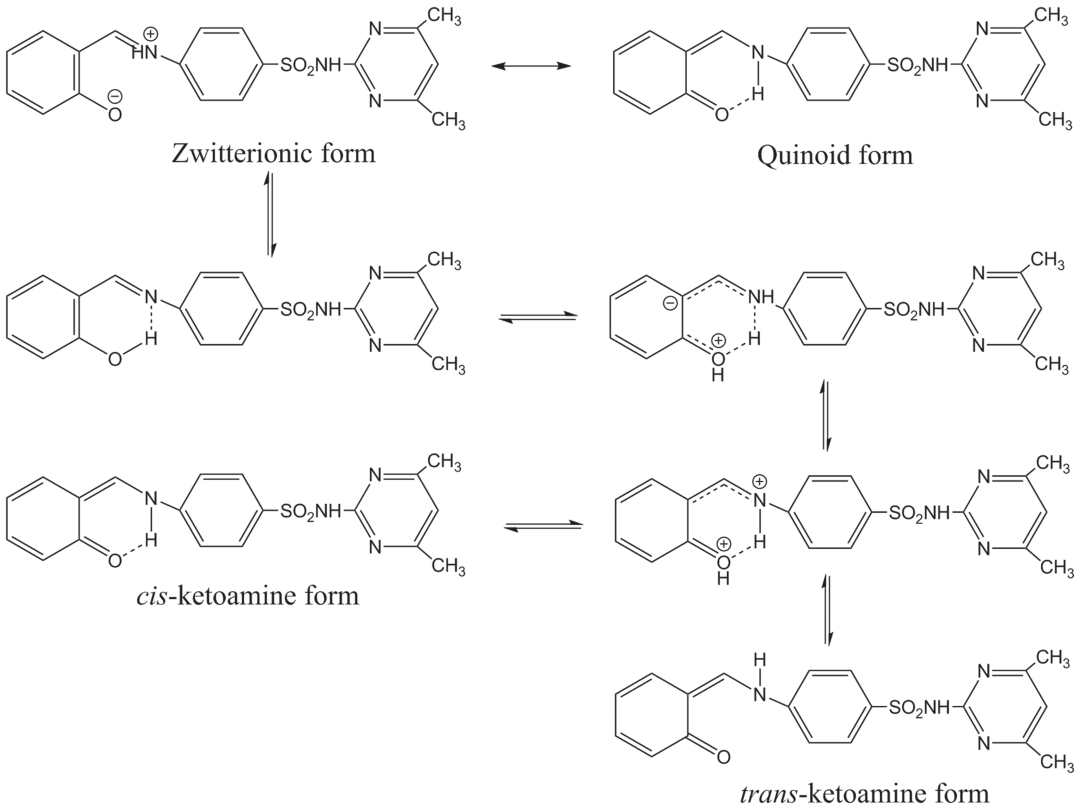

FIGURE 7 Enolimine-ketoamine tautomerism of $\mathbf{HL^1}$ in DMSO-d6

[Zn ($\mathbf{HL^2}$)$_2$(OAc)$_2$], [Zn ($\mathbf{HL^3}$)(OAc)$_2$].2H$_2$O and [Zn ($\mathbf{HL^4}$)(OAc)$_2$] .2H$_2$O exhibited abroad and low-intensity signal at δ 12.65, 9.65, 9.65 ppm, respectively, due to the phenolic-OH. Relative to the parent ligand, the latter signal was downfield shifted by (Δδ = 0 to + 0.13 ppm). This signal disappeared in the presence of D$_2$O and its broadness and low intensity could be considered as an evidence for bonding of the oxygen atom of the deprotonated and non-ionized phenolic group to the zinc (II) ion.[36] The [Zn ($\mathbf{HL^2}$)$_2$(OAc)$_2$], [Zn ($\mathbf{HL^3}$)(OAc)$_2$].2H$_2$O and [Zn ($\mathbf{HL^4}$)(OAc)$_2$].2H$_2$O complexes exhibited new signals at δ 3.30, 3.44 and 3.49 ppm, respectively, assignable to Zn (II) coordination. Methyl substituents in zinc complexes appeared at δ 2.40–2.51 ppm, whereas the sulfonamide (SO$_2$NH) proton resonated at δ 5.94–5.97 ppm and the signal disappeared with D$_2$O. The pyrimidine proton(s) signal appeared at δ 6.68–6.25 ppm. Other aromatic protons appeared at δ 6.55–8.54 ppm without coordination to the zinc ion as predicted from their chemical shifts.

3.1.5 | EPR spectra

The X-band EPR parameters of [Cu($\mathbf{L^1}$)(OAc)], [Cu($\mathbf{L^2}$)(OAc)] and [Cu($\mathbf{L^4}$)(OAc)].3H$_2$O showed rhombic nature of $g_3 > g_2 > g_1$ with g_{av} = 2.18, 2.15 and 2.14, respectively, demonstrating that the unpaired electron presents mainly in $d_{x^2-y^2}$ ground state confirming elongated tetragonally distorted copper geometry. Moreover, the R values, indicated the distortion towards symmetry of mixed $d_{x^2-y^2}$ and d_{z^2} states with increasing d_{z^2} predominance in their ground states than $d_{x^2-y^2}$. The spectrum of the polycrystalline sample [Cu($\mathbf{L^3}$)(OAc)] displayed axial parameters $g_{\|}$(2.27) > $g_{\perp}$(2.07)>g_e (2.0023) indicating $d_{x^2-y^2}$ ground state, and the latter was further confirmed by the 2.13 average g-value. The value of G- parameter, 3.80, indicated a negligible or very small direct Cu-Cu interaction in the solid-state and intermediate ligand field. In the parallel region, the spectrum displayed a hyperfine structure owing to the coupling of the nuclear spin (I = 3/2) of both copper isotopes ^{65}Cu and ^{63}Cu with the unpaired electron. The appearance of the parallel hyperfine revealed a covalent Cu-ligand bond. On the other hand, no splitting was observed in the $g_{\perp}$ region owing to the unresolved ligand hyperfine interaction at room temperature. As appeared from the spectrum, the hyperfine line splitting factor of 103G agrees with distortion from planarity. The tetragonal distortion was deduced from the empirical factor $f = g_{\|}/A_{\|}$ (220 cm^{-1}), in general, the value of $f \geq 150$ cm^{-1} revealed a strong distortion ascribed to the flexible structure

and/or bulkiness effect of the ligand. The planarity distortion towards the tetragonally distorted tetrahedral or octahedral structure decreased $A_{\parallel}$ and increased $g_{\parallel}$ as exemplified in many synthetic and biologically active copper compounds.[36,37]

Based on equation (9) the in-planar π bonding parameter α^2 was calculated to be 0.57 which agrees with covalent Cu-in-plane-ligand bonding and is inconsistent with the value of $g_{\parallel} < 2.30$.

$$\alpha^2 = A_{\parallel}/0.036 + \left(g_{\parallel} - 2.0023\right) + 3/7\left(g_{\perp} - 2.0023\right) + 0.04 \quad (9)$$

The room temperature X-band EPR spectrum of [Cu(**L**^{5})(OAc)].2H_2O showed an isotropic intense absorption band in the high field due to the tumbling motion of molecules[38] and the line width estimated from the spectrum $\Delta_{peak\text{-}peak}$ = 191 G. The g_i = 2.12 region indicated a dipole–dipole and weak exchange interactions between Cu (II) centers. The complex has low g-value signifying more covalent polar bonding. The g-value of 2.12 (> 2.0023 for the free electron) indicated the location of the unpaired electron predominantly in the $d_{x^2\text{-}y^2}$ orbital ground state. In general, the spectrum is consistent with the tetragonally distorted species with coordination number 4, in agreement with the literature data for distorted square planar copper complexes.[39]

3.1.6 | Thermal studies

Thermal analysis, Table 4, of the ligands and their complexes were studied utilizing thermogravimetric analysis (TGA), derivative thermogravimetric analysis (DTG), differential thermal analysis (DTA) and differential scanning calorimetric (DSC) methods in a stream of nitrogen and the results are compiled in the supporting information (Table S2). Furthermore, the % weight losses during decomposition steps are summarized and estimated in terms of the molecular formula. The TGA profiles and data of the ligands **HL**^{1}–**HL**^{5} showed two main decomposition steps except for **HL**^{3} which display three successive decomposition steps where each one displays maximum DTG peaks at which the degradation temperature occurred. The gradual degradation of ligands was accompanied by successive endothermic and exothermic DTA peaks and the heat capacity was calculated from the DSC curve.

The TGA profile of the copper complexes [Cu(**L**^{1})(OAc)] and [Cu(**L**^{2})(OAc)] proceeded in four degradation steps while [Cu(**L**^{3})(OAc)], [Cu(**L**^{4})(OAc)].3H_2O and [Cu(**L**^{5})(OAc)].2H_2O decomposed in three successive steps. The proposed fragments for the degradation steps are compiled in Table 4 All copper complexes displayed two endothermic and exothermic DTA peaks and the heat capacity values were calculated from the DSC curves, curves given in the supporting information (Table S2).

The TGA/DTA curves of [Zn(**L**^{1})]$_2$.2H_2O, [Zn (**HL**^{2})$_2$(OAc)$_2$], [Zn (**HL**^{3})(OAc)$_2$].2H_2O and [Zn (**HL**^{4})(OAc)$_2$].2H_2O complexes, as shown in the supporting information (Figure S3), exhibited three decomposition steps, while, on the other hand, [Zn(**L**^{5})$_2$] complex displayed degradation within two steps. The residual decomposition products in all zinc complexes were ZnO as remains. The DTA curve of [Zn(**L**^{1})]$_2$.2H_2O and [Zn (**HL**^{2})$_2$(OAc)$_2$] complexes showed two endothermic peaks and one exothermic peak, however, other complexes of **HL**^{3}-**HL**^{5} displayed an endothermic and an exothermic peak. The heat capacity for the zinc complexes was calculated from the DSC curve. The thermal studies of the synthesized complexes from their curves were in good agreement with their proposed structures and their molecular formula.

The thermodynamic parameters of decomposition namely, activation energy (E_a), enthalpy change (ΔH), entropy change (ΔS) were evaluated by employing the Horowitz-Metzger equation,[40] and given in the supporting information (Table S2). The chemical reaction order (n) and the value of the decomposed substance fraction (α_m) were calculated utilizing the Kissinger method.[41] The values of collision factor (Z) was obtained using Horowitz-Metzger equation (10),[40]

$$Z = \frac{E_a}{RT_m}\phi \exp\left(\frac{E_a}{RT_m^2}\right) = \frac{KT_m}{h}\exp\left(\frac{\Delta S}{R}\right) \quad (10)$$

where (ΔS) is the entropy of activation, (R) represents molar gas constant, (ϕ) rate of heating (K S^{-1}), (K) the Boltzmann constant, and (h) the Planck's constant.[42] The change in enthalpy (ΔH) for any phase proceeding at any peak temperature (T_m), was determined from the relation (ΔS = ΔH/T). Considering, the least square calculations, the lnT against 1,000/T plots for all complexes, for DTA curve, gave straight lines from which the activation energies are calculated according to the stated method.[42] The slope is of Arrhenius type and equals to (− E_a/R).

The heat capacity (C_p) could be calculated from the relation (11):

$$C_p = \frac{Q}{\Delta T} \quad (11)$$

where (C_p) is the heat capacity in ($mJ.g^{-1}\ K^{-1}$) and (Q) is the amount of heat energy or heat flow per unit of time (mJ/sec) and (ΔT) is the temperature differences between the onset and the offset of the endothermic and exothermic peaks. The calculated heat capacity values are collected in the supporting information (Table S2).

Based on the thermal results, the following points are concluded:

- The calculated values of the collision number (Z) in each case exhibited a direct relation to (E_a). Both maximum and minimum (Z) values were 3.84 and 0.109, respectively, indicating variable mechanisms at different speeds.
- At the maximum development of the reaction in each step, the values of the decomposed fraction (α_m) have the same magnitude ranging from 0.72 to 0.40 within the melting temperature (T_m) range 862.3–352.7 K.
- The entropy change (ΔS) for all compounds is in the range of - 0.239 to - 0.271 $kJK^{-1}\ mol^{-1}$ indicating ordered transition states in less random molecular configurations than the complexes.
- The fraction values of the order of the reaction (n) suggested either incomplete reaction or its proceeds in a complicated mechanism.

The activation energies (E_a) of Cu (II) complexes are lower than that of Zn (II) complexes. The order is by the rule stated that: the activation energy (E_a) of the complex increases as the metal ion radius decreased (Zn (II) = 88 pm < *r* Cu (II) = 91 pm). The trend of the calculated (E_a, $kJmol^{-1}$) of the complexes using Horowitz-Metzger method at the first decomposition step is in the following order:

[Zn ($\mathbf{L^1}$)$_2$].2H_2O = 28.406 > [Cu($\mathbf{L^1}$) (OAc)] = 27.345, [Zn ($\mathbf{HL^2}$)$_2$(OAc)$_2$] = 61.414 > [Cu($\mathbf{L^2}$)(OAc)] = 41.911, [Zn ($\mathbf{HL^3}$)(OAc)$_2$].2H_2O = 36.117 > [Cu($\mathbf{L^3}$) (OAc)] = 28.644,[Zn ($\mathbf{HL^4}$)(OAc)$_2$].2H_2O = 60.951 > [Cu ($\mathbf{L^4}$)(OAc)].3H_2O = 41.564, [Zn($\mathbf{L^5}$)$_2$] = 33.688 > [Cu($\mathbf{L^5}$) (OAc)].2H_2O = 32.296.

- The negative (ΔH) values indicate an exothermic decomposition process.
- The heat capacity (C_p) of the dehydration process of the hydrated complexes is nearly similar and equals to 272.9 $mJg^{-1}\ K^{-1}$.

3.2 | Antimicrobial evaluation

The antimicrobial screening data Table 5, are represented graphically, in the supporting information (Figure S4). Results indicated that among the tested ligands, $\mathbf{HL^1}$ exhibited potent activity versus Gram-negative bacteria and the growth inhibition zone diameters were 22.6 mm (*E. Coli*), 18.3 mm (*P.Aeruginosa*). Interestingly, the inhibition zone diameters are higher than those obtained by the standard bacteriocide *Gentamicin.*

As reported in the literature, the discovery of potent antitumor candidates depends basically on the line of antibiotics affecting Gram-negative bacteria.[43,44] The membrane of these bacteria is surrounded by a lipopolysaccharides outer membrane which allows lipid-soluble materials passage. It is clear that $\mathbf{HL^1}$ combined with the lipophilic layer via charge transfer interaction and thus, enhanced the membrane permeability of the Gram-negative bacteria and it restricted further growth of the organisms.[45] $\mathbf{HL^2}$ exhibited potent activity against Gram-positive bacteria like Gentamicin and Ampicillin; the standard bactericides in use. $\mathbf{HL^3}$ and $\mathbf{HL^4}$ virtually lack any noticeable antibacterial activity, while $\mathbf{HL^5}$ showed moderate activity against B. subtilis and S. pneumonia, low activity against E. Coli and inactive against P. aeruginosa. Concerning structure–activity correlation, it may be concluded that imines based salicylaldehyde exhibited higher activity than those derived from 2-hydroxynaphth- aldehyde.

Antibacterial activities of Cu (II) and Zn (II) complexes are given in Table 5. It is obvious that copper complexes are more active than zinc complexes. Noteworthy, [Cu($\mathbf{L^1}$)(OAc)] displayed a higher inhibition zone against *S. pneumoniae* and *B. subtilis* than the precursor ligand $\mathbf{HL^1}$. On the other hand, [Cu($\mathbf{L^2}$)(OAc)] exerted equal inhibition zone diameters as the standard bacteriocides in use. Analogously, [Cu($\mathbf{L^3}$)(OAc)] exhibited high activity against *B. subtilis* and it was also performed an inhibition zone diameter greater than *Ampicillin.*

Remarkably, all zinc complexes exhibited no activity only against *Pseudomonas aeruginosa*. Concerning metal-activity correlation, it was noticed that [Cu($\mathbf{L^2}$)(OAc)], [Cu($\mathbf{L^3}$) (OAc)], [Zn ($\mathbf{HL^3}$)(OAc)$_2$].2H_2O and [Zn ($\mathbf{HL^4}$) OAc)$_2$].2H_2O exerted higher activity compared to their ligands. In contrary, $\mathbf{HL^5}$ exhibited a better activity against all bacteria strains than its complexes. it was concluded that metal chelates enhanced the biological activity and this behavior could be explained in terms of azomethine H-bonding with various active cellular constituents that produce interference with normal cellular processes.[46]

The data of the antifungal activity of $\mathbf{HL^1}$-$\mathbf{HL^5}$ and their metal (II) complexes are collected in Table 5 and (in the supporting information Figure S4). It was shown that: (i) the free ligands displayed appreciable antifungal activity in the order: $\mathbf{HL^2 > HL^1 > HL^5 > HL^4 > HL^3}$. (ii) the [Cu($\mathbf{L^3}$)(OAc)] complex showed high potency

TABLE 5 Antimicrobial screening results of sulfonamide imine ligands and their Cu (II) and Zn (II) complexes

Inhibition zone diameter (mm/mg sample)						
Compound	*E. Coli ATCC 6538*	*P. Aeruginosa ATCC 9027*	*S. Pneumoniae ATCC 49619*	*B. subtilis ATCC 6633*	*C. albicans ATCC 10231*	*A. fumigatus ATCC 46645*
	(Gram negative bacteria)		***(Gram positive bacteria)***		***(Fungi)***	
Gentamicin(G-)	19.9	17.3				
Ampicillin (G+)			23.8	32.4		
Amphotericin B					25.4	23.7
Control: DMSO	Nil	Nil	Nil	Nil	Nil	Nil
HL^1	22.6	18.3	16.3	18.3	16.9	17.3
[Cu(**L^1**) (OAc)]	20.3	NA	18.2	20.3	17.2	21.3
[Zn (**L^1**)$_2$].2H$_2$O	11.9	NA	16.9	18.2	13.8	15.7
HL^2	19.9	17.3	23.8	32.4	19.6	20.2
[Cu (**L^2**)(OAc)]	19.9	17.3	23.8	32.4	25.4	23.7
[Zn (**HL^2**)$_2$(OAc)$_2$]	10.8	NA	12.9	13.2	16.9	18.7
HL^3	NA	NA	NA	NA	11.2	12.6
[Cu (**L^3**) (OAc)]	18.3	13.1	22.6	33.7	17.6	24.3
[Zn (**HL^3**) (OAc)$_2$].2H$_2$O	18.9	NA	17.5	19.8	13.4	15.3
HL^4	NA	NA	NA	NA	13.3	15.7
[Cu(**L^4**) (OAc)].3H$_2$O	17.6	12.3	19.5	29.8	16.5	22.3
[Zn (**HL^4**) (OAc)$_2$].2H$_2$O	8.5	NA	12.3	12.7	15.4	17.6
HL^5	13.6	NA	16.7	19.2	15.9	16.8
[Cu (**L^5**) (OAc)].2H$_2$O	11.2	NA	10.2	9.8	15.9	14.6
[Zn (**L^5**) $_2$]	9.4	NA	14.6	14.3	11.7	13.6

NA = No Activity.

against *Aspergillus fumigatus* and it even displayed higher activity than *Amphotericin B,*(iii) analogously, [Cu(**L^2**)(OAc)] possessed more potent activity than its parent ligand and it displayed similar activity like the fungicide in use, (iv) metal chelates have higher activity than free ligands and this may be clarified in terms of chelation theory and overtone's concept.[47] The complexes increased the lipophilicity and thus, enhanced the penetration into lipid membranes and blocked the sites on the enzymes of the microorganism, (v) the activity of the complexes versus different organisms relies on either the differences in ribosome in microbial cells or the impermeability of the microbe's cells.[46]

The free **HL^1**, as well as the complexes [Cu(L^2)(OAc)] and [Cu(L^3)(OAc)], were selected to determine the minimum inhibitory concentration (MIC) for antibacterial activity[48] and the MIC (μg / mL) results are given in Table 6. The [Cu(**L^2**)(OAc)] complex exhibited high activity against *B. subtilis* (MIC = 0.4 μg / mL), *E. Coli* and *S. Pneumonia* (MIC = 1.95 μg/mL) and *P. Aeruginosa* (MIC = 7.81 μg/mL).

3.3 | In vitro cytotoxicity assessment

Searching for novel metal complexes like *cis*-diaminodichloro platinum (II) (cisplatin) for cancer treatment has witnessed a growing research interest and a great number of even non-platinum complexes exhibit remarkable activity in this concern.[22,49,50] The antitumor studies of **HL^1**, [Cu(**L^2**)(OAc)] and [Cu(**L^3**)(OAc)] were estimated versus liver cancer (HEPG2), breast

TABLE 6 Minimum inhibitory concentrations (MIC) in (μg/mL) for antibacterial activity

Compound	*E. Coli ATCC 6538* *(Gram negative)*	*P.Aeruginosa ATCC 9027*	*S.Pneumonia ATCC 49619* *(Gram positive)*	*B.subtilis ATCC 6633*
Streptomycin *(Gram negative)*	0.03	3.9		
Penicillin G *(Gram positive)*			0.06	0.03
HL^1	31.25	62.5	62.5	31.25
[Cu (L^2)(OAc)]	1.95	7.81	1.95	0.49
[Cu (L^3)(OAc)]	7.81	15.63	7.81	3.9

TABLE 7 IC_{50} values (μg/ml) in Doxorubicin as standard for **HL^1**, [Cu (L^{2-3}) (OAc)] against HEPG2, MCF7 and HCT 116 (doses ranging from 0 to 50 μg/ml)

Compound	MCF-7 (Breast carcinoma)	HCT-116 (Colon carcinoma)	HEPG-2 (Hepatocellular)
Doxorubicin	0.44	0.47	1.2
HL^1	15.5	9.6	16.2
[Cu (L^2)(OAc)]	6.2	7.4	9.1
[Cu (L^3) (OAc)]	6.9	12.5	4.8

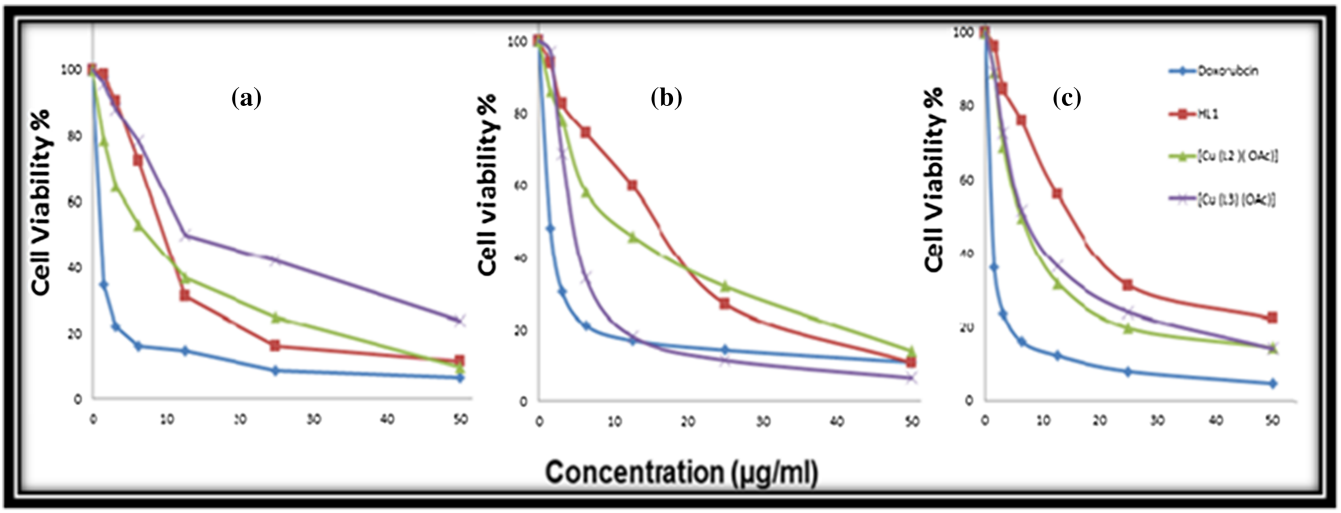

FIGURE 8 Plot of cell viability % versus concentration of **HL^1** ligand, [Cu(L^2)(OAc)] and [Cu (L^3)(OAc)] against: a) HCT-116, b) HEPG-2, c) MCF-

cancer (MCF7) and colon cancer (HCT 116) as well as the IC_{50} values using doxorubicin as a standard are listed in Table 7 and shown in Figure 8. The [Cu (**L^3**)(OAc)] exhibited higher activity versus HEPG-2 than other cell lines; IC_{50} = 4.8 μg/ml. Noteworthy, the [Cu(**L^2**)(OAc)] exhibited potent activity against breast carcinoma MCF-7 and colon carcinoma; IC_{50} = 6.2, 7.4 and 9.1 μg/ml, respectively. These results might be recommended as new findings of promising antitumor candidates for clinical and experimental chemotherapy.

4 | CONCLUSIONS

The targeted well-separated spherical nanosized ligands **HL^1**-**HL^5** were prepared. The heating ethanolic solution of copper or zinc acetates with an equimolar ratio of the appropriate ligands furnished the corresponding complex. ^{1}H-NMR spectrum of **HL^1**, as a representative example, indicated the presence of four isomers in (8:5:2:1) ratios attributed to enol-imine-keto-amine tautomerism in DMSO, the enol tautomer was observed as a

resonance hybrid of two canonical structures, the zwitterionic and/or quinoid forms, while the keto-amine tautomer is regarded as *trans* or *cis* relative to the C=N bond. The absence of phenolic-OH signal in $[Zn(\mathbf{L^1})_2].2H_2O$ and $[Zn(\mathbf{L^5})_2]$ confirmed its deprotonation upon complexation. Other zinc complexes exhibited phenolic-OH, disappeared upon D_2O treatment, unambiguously proved to bond to zinc (II) ion.

The optimized geometries of $\mathbf{HL^1}$-$\mathbf{HL^5}$ ligands were verified by performing time-dependent density functional analysis (TD-DFT). Quantum chemical parameters including energy gap, absolute electronegativities, chemical potentials, absolute hardness, absolute softness, global electrophilicity, global softness, an additional electronic charge of the ligands $\mathbf{HL^1}$- $\mathbf{HL^5}$ were calculated.

The antimicrobial screening results against various pathogenic bacteria revealed a unique potent activity of $\mathbf{HL^1}$ against Gram-negative bacteria and exhibited efficient potential higher than the standard *Gentamicin*. The $[Cu(\mathbf{L^1})(OAc)]$ and $[Cu(\mathbf{L^3})(OAc)]$ complexes displayed better activity compared to standard bacteriosides in use. It was noticed that $[Cu(\mathbf{L^2})(OAc)]$, $[Cu(\mathbf{L^3})(OAc)]$, $[Zn\ (\mathbf{HL^3})(OAc)_2]$ and $[Zn\ (\mathbf{HL^4})OAc)_2]$ exerted higher activity compared to their ligands. The minimum inhibitory concentration (MIC) of $[Cu(\mathbf{L^2})(OAc)]$ exhibited high activity against *B. subtilis* (0.4 μg/mL), *E. Coli* and *S. Pneumonia* (1.95 μg/mL) and *P. Aeruginosa* (7.81 μg/mL). in vitro antitumor studies, $[Cu(\mathbf{L^3})(OAc)]$ exhibited remarkable activity against HEPG-2 (IC_{50} = 4.8 μg/ml). The $[Cu(\mathbf{L^2})(OAc)]$ showed potent activity against MCF-7 and HCT 116 (IC_{50} = 7.4 and 9.1 μg/ml). These results might be recommended as new findings of promising antitumor candidates for clinical and experimental chemotherapy.

CONFLICT OF INTEREST

The authors declare that no conflict of interest.

AUTHOR CONTRIBUTIONS

Ali El-Dissouky: Methodology; project administration; supervision. **Eslam S. Abu-Elsoud:** Formal analysis; investigation. **Afaf Abdel Razik:** Formal analysis; investigation. **Mohamed K. Awad:** Data curation; software; validation. **Hammed H.A.M. Hassan:** Formal analysis.

ORCID

Amel F. Elhusseiny https://orcid.org/0000-0001-6395-5742

REFERENCES

[1] H. M. Dalloul, K. N. El–Nwairy, A. Z. Shorafa, A. S. A. Samaha, *MOJ Biorg. Org. Chem.* **2017**, *1*, 255. https://doi.org/10.1155/S1565363303000244

[2] a) M. K. Gupta, H. L. Singh, S. Varshney, A. K. Varshney, *Bioinorg. Chem. Appl.* **2003**, *1*, 34. b) S. K. Adavi, A. A. Yadav, R. S. Bendre, *J. Mol. Str.* **2018**, *1152*, 223.

[3] C. S. Allardyce, P. J. Dyson, *Dalton Trans.* **2016**, *4*, 3201. https://doi.org/10.1039/C5DT03919C

[4] D. P. Pate, S. P. Prajapati, A. K. Rana, P. S. Patel, *Pelagia Research Library* **2012**, *3*, 491.

[5] J. Osredkar, N. Sustar, *J. Clinic.Toxicol.* **2011**, *S*: 3.

[6] T. J. McCarthy, J. J. Zeelie, D. J. Krause, *Clin. Pharma. Ther.* **1992**, *17*, 5.

[7] L. Leinartaite, K. Saraboji, A. Nordlund, D. T. Logan, M. Oliveberg, *J. Am. Chem. Soc.* **2010**, *132*, 13495. https://doi.org/10.1021/ja1057136

[8] N. Fabris, E. Mocchegiani, *Aging* **1995**, *7*, 77. https://doi.org/10.1007/BF03324297

[9] M. Araya, F. Pizarro, M. Olivares, M. Arredondo, M. González, M. Méndez, *Biol. Res.* **2006**, *39*, 183. https://doi.org/10.4067/s0716-97602006000100020

[10] Y. Christen, *Am. J. Clin. Nutr.* **2000**, *71*, 621S. https://doi.org/10.1093/ajcn/71.2.621s

[11] B. K. Bitanihirwe, M. G. Cunningham, *Synapse* **2009**, *63*, 1029. https://doi.org/10.1002/syn.20683

[12] a) S. J. Lippard, J. M. Berg, *Principles of bioinorganic chemistry*, University Science Books, Mill Valley, California **1994**. ISBN 0-935702-73-3 b) E. D. Harris, *Nutr. Rev.* **2001**, *59*, 281. https://doi.org/10.1111/j.1753-4887.2001.tb07017.x

[13] C. Pichot, reactive nanocolloids for nanotechnologies and microsystems, in *colloidal nanoparticles in biotechnology*, (Ed: A. Elaissari), wiley-interscience a john wiley & sons, inc., publication **2008** 1.

[14] M. Gaber, H. A. El-Ghamry, S. K. Fathalla, M. A. Mansour, *Mater. Sci. & Eng. C.* **2018**, *83*, 78.

[15] T. L. Riss, R. A. Moravec, *Assay Drug Dev. Technol.* **2004**, *2*, 51. https://doi.org/10.1089/154065804322966315

[16] A. D. Becke, *J. Chem. Phys.* **1993**, *98*, 5648. https://doi.org/10.1063/1.464913

[17] P. C. Hariharan, J. A. Pople, *Theoret. Chim. Acta* **1973**, *28*, 213. https://doi.org/10.1007/BF00533485

[18] M. J. Frisch, et al, Gaussian 03. Revision B.01. Gaussian. Inc. Pittsburgh PA, **2003**.

[19] T. L. Decker, M. L. Lohmann-Matthes, *J. Immunol. Method* **1988**, *115*, 61. https://doi.org/10.1016/0022-1759(88)90310-9

[20] H. H. A. M. Hassan, E. M. E. Mansour, A. M. S. A. Zeid, E. R. El-Helow, A. F. Elhusseiny, R. Soliman, *Che. Cent. J* **2015**, *9*, 44. https://doi.org/10.1186/s13065-015-0123-2

[21] G. M. G. Hossain, A. J. Amoroso, A. Banu, K. M. A. Malik, *Polyhedron* **2007**, *26*, 967. https://doi.org/10.1016/j.poly.2006.09.056

[22] A. F. El Husseiny, A. El-Dissouky, A. M. H. Al-Hamza, H. A. M. Hassan, *J. Coord. Chem.* **2015**, *68*, 241. https://doi.org/10.1080/00958972.2014.982551

[23] R. Dennington, T. Keith, J. Millam, Gauss View, Version 4.1.2, Semichem Inc., Shawnee Mission, KS. Google Scholar, **2007**.

[24] W. H. Mahmoud, R. G. Deghadi, M. M. I. El Desssouky, G. G. Mohamed, *Appl. Organometal Chem.* **2019**, *33*, e4556. https://doi.org/10.1002/aoc.4556

[25] R. A. Bhat, D. Kumar, A. Alam, B. A. Mir, A. Srivastava, M. A. Malla, M. A. Mir, *J. Mol. Str.* **2018**, *1173*, 72. https://doi.org/10.1016/j.molstruc.2018.06.061

[26] G. G. Mohamed, M. A. Zayed, S. M. Abdallah, *J. Mol. Str.* **2010**, *979*, 62. https://doi.org/10.1016/j.molstruc.2010.06.002

[27] M. A. Arafath, F. Adam, M. R. Razali, L. E. A. Hassan, M. B. K. Ahamed, A. M. Majid, *J. Mol. Str.* **2017**, *1130*, 791.
[28] A. F. Elhusseiny, E. S. Aazam, H. M. Al-Amri, *Spectrochim. Acta Part A* **2014**, *128*, 852. https://doi.org/10.1016/j.saa.2014.03.003
[29] M. A. EL-Nawawy, R. S. Farag, I. A. Sabbah, A. M. Abu–Yamin, *IJPSR* **2011**, *2*, 3143. https://doi.org/10.13040/IJPSR.0975-8232
[30] A. B. P. Lever, *Coord. Chem. Reviews* **1968**, *3*, 119. https://doi.org/10.1016/S0010-8545(00)80107-1
[31] a) R. Karbouje, A El-Dissouky, E Al-Saleh, B Jeragh, *J. Coord. Chem.* **2010**, *63*, 868. https://doi.org/10.1080/00958971003645946 b) L. A. Saghatforoush, S. Hosseinpour, M. W. Bezpalko, W. S. Kassel, *Inorg. Chim. Acta* **2019**, *484*, 527. https://doi.org/10.1016/j.ica.2018.04.053
[32] J. Matijević-Sosa, M. Vinković, D. Vikić-Topić, *Croat. Chem. Acta* **2006**, *79*, 489. https://hrcak.srce.hr/5662
[33] E. S. Aazam, A. Fawazy, P. B. Hitchcock, *Acta Crystallogr. E* **2006**, *62*, o4285. https://doi.org/10.1107/S1600536806034519
[34] R. J. Santos-Contreras, A. Ramos-Organillo, E. V. García-Báez, I. I. Padilla-Martínez, F. J. Martínez-Martínez, *Acta Crystallogr. C.* **2009**, *65*, o8. https://doi.org/10.1107/S0108270108040407
[35] A. A. Emara, A. A. Saleh, O. M. I. Adly, *Spectrochim. Acta Part A* **2007**, *68*, 592. https://doi.org/10.1016/j.saa.2006.12.034
[36] A. F. Elhusseiny, H. H. A. M. Hassan, H. Hussien, A. El-Dissouky, R. A. Palmer, J. K. Cockcroft, *Transition Met. Chem.* **2015**, *40*, 643. https://doi.org/10.1007/s11243-015-9958-6
[37] B. K. Singh, U. K. Jetley, R. K. Sharma, B. S. Garg, *Spectrochim. Acta A* **2007**, *68*, 63. https://doi.org/10.1016/j.saa.2006.11.001
[38] a) M. S. Masoud, E. A. Khalil, A. M. Hafez, A. F. El-Husseiny, *Spectrochim. Acta A* **2005**, *61*, 989. https://doi.org/10.1039/B417739H b) A. C. Warden, L. Spiccia, M. T. W. Hearn, J. F. Boas, J. R. Pilbrow, *Dalton* **2005**, *10*, 1804.
[39] A. F. Elhusseiny, H. Hussien, H. H. A. M. Hassan, *Lett. Org. Chem.* **2019**, *16*, 235.
[40] H. H. Horowitz, G. A. Metzger, *Anal. Chem.* **1963**, *35*, 1464. https://doi.org/10.1021/ac60203a013
[41] E. Kissinger, *Anal. Chem.* **1957**, *29*, 1702. https://doi.org/10.1021/ac60131a045
[42] M. L. Dhar, O. Singh, *J. Therm. Anal.* **1991**, *37*, 259. https://doi.org/10.1007/BF02055928
[43] H. Nikaido, T. Nakae, *Adv. Microbiol. And Phys.* **1979**, *20*, 163. https://doi.org/10.1016/S0065-2911(08)60208-8
[44] M. Abdul Qadir, M. Ahmed, H. Aslam, S. Waseem, M. I. Shafiq, *J. Chem.* **2015**, *2015*, 1. https://doi.org/10.1155/2015/524056
[45] F. Barbato, V. Cirocco, L. Grumetto, M. I. La Rotonda, *Eur. J. Pharm. Sci.* **2007**, *31*, 288. https://doi.org/10.1016/j.ejps.2007.04.003
[46] A. F. Elhusseiny, A. El-Dissouky, A. M. Al-Hamza, H. H. A. M. Hassan, *J. Mol. Str.* **2015**, *1100*, 530. https://doi.org/10.1016/j.molstruc.2015.07.049
[47] B. G. Tweedy, *Phytopathology* **1964**, *55*, 910.
[48] S. Jayakumar, D. Mahendiran, D. Arumai Selvan, A. Kalilur Rahiman, *J. Mol. Str.* **2019**, *1196*, 567. https://doi.org/10.1016/j.molstruc.2019.06.088
[49] A. F. Elhusseiny, H. H. A. M. Hassan, *Spectrochim. Acta A.* **2013**, *103*, 232. https://doi.org/10.1016/j.saa.2012.10.063
[50] Y. Kwon, J. Song, H. Lee, E. Kim, K. Lee, S. Lee, S. J. Kim, *Med. Chem.* **2015**, *58*, 7749. https://doi.org/10.1021/acs.jmedchem.5b00764

SUPPORTING INFORMATION

Additional supporting information may be found online in the Supporting Information section at the end of this article.

How to cite this article: El-Dissouky A, Abu-Elsoud ES, Abdel Razik A, Awad MK, Hassan HHAM, Elhusseiny AF. Synthesis, molecular modeling, TD-DFT, antimicrobial, and in vitro therapeutic activity of new spherical nano-sized sulfonamide imine ligands and their zinc (II) and copper (II) complexes. *Appl Organomet Chem*. 2020;e5953. https://doi.org/10.1002/aoc.5953